NTNU
Faculty of Natural Sciences
Department of Chemical Engineering

Evaluation of different block-copolymers coatings of iron oxide nanoparticles by flash nanoprecipitation

Felix Bogdan

Master Thesis in N5T Polymer Technology

NTNU:
Supervisor: Assoc. Prof. Dr. Sulalit Bandyopadhyay
Co-supervisor: M.Sc. Nesrine Bali

KTH:
Supervisor: Prof. Dr. Eva Malmström Jonsson

June 23, 2023
Trondheim

Acknowledgments

This work has been performed at the Department of Chemical Engineering at Norges teknisk-naturvitenskapelige universitet – NTNU. As part of the Particle Engineering Centre (PEC) I got the opportunity to connect the fields of nanotechnology, polymer science and chemical engineering in an independent work. I want to always thank Sulalit for his support and scientific inputs throughout the project. I want to extend a special thanks to Nesrine, who has been instrumental in providing invaluable assistance in the lab and with research matters. I would like to express my gratitude to my fellow students, Solveig, Sigrid, and Camillo, for greatly simplifying my life both in the lab and office.

I must not forget to mention the consistently positive feedback on all my results and slides presented received from Eva at KTH. Her unwavering positivity has been a source of motivation and encouragement throughout this project.

I confirm that I have independently completed the work without any external assistance and without using sources other than those specified. Furthermore, I confirm that the work has not been submitted to any other examination board in the same or similar form and has been accepted by this board as part of an examination. All direct or indirect quotations that have been adopted are identified as such.

23. June 2023 — Date

Felix Bogdan — Signature

Abstract

Nanoparticles (NPs) offer unique possibilities for medical applications, including the controlled release of cancer drugs, the use as imaging contrast during imaging procedures or the hyperthermic treatment of cancer cells. Flash Nanoprecipitation (FNP) produces NPs to combine these applications in a fast, cheap, and scalable coating process. Until now, FNP was successfully used to encapsulate hydrophobic, organic anti-cancer drugs with block-copolymers [1, 2]. The combination of hydrophobic oleic acid iron oxide NPs (IONPs) with amphiphilic block-copolymers offers promising theranostic abilities when modified with targeting ligands [3]. The use of FNP with a Multi Inlet Vortex Mixer (MIVM) is a promising method to easily coat IONPs with block-copolymers. The FNP coating process needs yet to be tested and understood for various biocompatible block-copolymers (Figure 1).

Amphiphilic block-copolymers based on hydrophilic polyethylene glycol (PEG) and hydrophobic poly(lactic acid) (PLA), poly(lactic-co-glycolic acid) (PLGA) or poly(caprolactone) (PCL) were successfully synthesized. The organic catalyst 1,8-diazabicyclo[5.4.0]undec-7-ene (DBU) was used to increase biocompatibility of the resulting polymers PEG-PLA, PEG-PLGA and PEG-PCL. The synthesis of hydroxyl terminated poly(acrylic acid) (PAA-OH) followed by the polymerization with PLGA was attempted.

The amphiphilic block-copolymers were used in combination with the stabilizer polysorbate 80 (Tween80) in FNP to form bare polymeric NPs using a MIVM as the reactor. DLS and STEM confirmed particle sizes between 50-100 nm. The addition of 13 ± 2 nm hydrophobic oleic acid coated IONPs yielded an increase in particle size as well as increase in particle stability over time. STEM images showed attachment of single IONPs to the outside of the polymeric NPs. Hydrophobic interactions between the polymer and oleic acid coated IONPs are possible.

To achieve encapsulation of the IONPs, adjustments to the process parameters of FNP should be considered in future research. Additional experiments are required to explore possible drug addition, release mechanisms and hyperthermia behavior of the polymer coated IONPs particles.

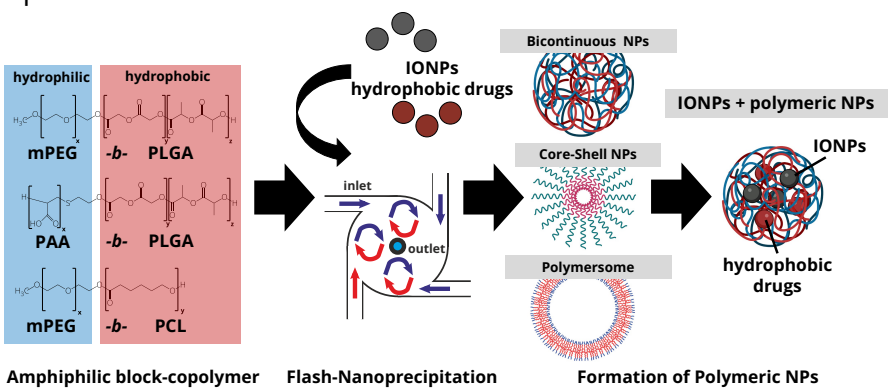

Figure 1: Graphical Abstract: Synthesis of biocompatible block-copolymers followed by the fabrication of polymeric nanoparticles and addition of hydrophobic oleic acid through FNP.

Table of Contents

Table of Abbreviations

AAc		acrylic acid
AAP		activated alcohol pathway
AIBN		azobis(isobutyronitril)
API		active pharmaceutical ingredients
ATR		attenuated total reflectance
$CHCL_3$		chloroform
CIJ		confined impinging jet
CL		ε-caprolactone
CNC		critical nucleation concentration
$Đ_m$		dispersity of polymer M_w/M_n
DBU		1,8-Diazabicyclo[5.4.0]undec-7-ene
DCM		dichloromethane
DMSO		dimethylsulfoxide
DP		degree of polymerization
DLS		dynamic light scattering
DSC		differential scanning calorimetry
EMA		European Medicines Agency
FDA		Food and Drug Administration
FNP		flash nanoprecipitation
FTIR		Fourier-transform infrared spectroscopy
GA		glycolic acid or glycolide
GPC		gel permeation chromatography
HSP		Hansen solubility parameter
IONPs		iron oxide nanoparticles
LA		lactic acid or rac-lactide
ME		2-Mercaptoethanol
MIVM		multi inlet vortex mixer
M_n	g/mol	number average molecular weight
MQ		deionized water
M_w	g/mol	weight average molecular weight
mPEG		methyl-poly(oxyethylene)
NAP		nucleophilic attack pathway
NMR		nuclear magnetic resonance
NPs		nanoparticles
OA		oleic acid
PAA-OH		hydroxyl terminated poly(acrylic acid)
PAA-PLGA		poly(acrylic acid)-b-poly(lactic-co-glycolic acid)
PAA-PS		poly(acrylic acid)-b-poly(styrene)

PCL		poly(caprolactone)
PDI		polydispersity index
PEG		poly(ethylene glycol)
PEG-PCL		poly(ethylene glycol)-b-poly(caprolactone)
PEG-PLA		poly(ethylene glycol)-b-poly(lactic acid)
PEG-PLGA		poly(ethylene glycol)-b-poly(lactic-co-glycolic acid)
PEG-PSS		poly(ethylene glycol)-*b*-poly(propylene sulfide)
PGA		poly(glycolic acid)
PLA		poly(lactic acid)
PLGA		poly(lactic-co-glycolic acid)
Re		Reynolds number
ROP		ring opening polymerization
RT		room temperature
S		supersaturation
$Sn(Oct)_2$		stannous octoate
S(T)EM		scanning transmission electron microscope
t_{agg}	s	aggregation time in flash nanoprecipitation
t_{mix}	s	mixing time in flash nanoprecipitation
$t_{nuc,gro}$	s	nucleation and growth time in flash nanoprecipitation
T_g	K	glass transition temperature
T_m	K	melting temperature
TGA		thermogravimetric analysis
THF		tetrahydrofuran
Tween80		Polysorbate 80 - Polyoxyethylene (20) sorbitan monooleate

List of Figures

List of Tables

1. Introduction

When the size of a material is decreased from the macroscale to the nanoscale, the relative surface area of the material increases. This is one important factor that leads to changes in the magnetic, optical, electrical, and thermal properties of the material. One example of such unique properties is the localized surface plasmon of noble metal nanoparticles (NPs), which is used in biomedical sensing applications. Addition of metal NPs can increase the thermal conductivity of certain fluids, while addition of extremely hard NPs to lubricants can lower the friction between gears [4]. The fabrication of NPs with a size of <100 nm is important for a wide range of commercial applications. Some of the most prominent include the metal-based nanoparticles made of titanium dioxide, zinc oxide and silver. The application of these particles include antibacterial coating, food additives and UV protection in cosmetic products [5]. Besides these inorganic NPs, other classes include organic NPs (polymeric NPs) and biology-based NPs. To utilize the full potential of different material classes, hybrid nanoparticles can be produced which can combine organic and inorganic materials. A combination of properties in such hybrid NPs can have synergetic effects and allow one particle to act in a variety of different applications. [6, 7]

The combination of two materials metal-based core and polymeric shell can yield promising hybrid NPs for biomedical application. Iron oxide NPs (IONPs) can be used to induce hyperthermia, release drugs at target specific tissue and/or act as contrast agent [8]. The polymer shell acts as transport agent reduces toxicity of the iron core, increases the bioavailability, and enables prolonged stability in vivo. The shell can be modified to suppress certain interaction, while facilitating other processes and interactions with cells. Highly optimized hybrid metal – polymer systems could be used for treatments of various diseases, including cancer. [9]

Synthesis of these NPs systems can be a challenge, because of cost intensive and complex fabrication pathways. Flash nanoprecipitation (FNP) is a one-step process yielding monodisperse polymeric NPs in an aqueous solution by rapid mixing in confined impingement jet (CJI) or multi-inlet vortex mixer (MIVM) reactors. The mixing of a water-soluble organic phase and an aqueous water phase results in fast diffusion of the organic phase into the aqueous phase during FNP. Low water components present in the organic phase experience high supersaturation (S) followed by rapid nucleation and growth. Amphiphilic block-copolymer and/or stabilizers hinder the particle growth and prevent aggregation. By varying type and amount of polymers, the NPs can be modified to address different applications and improve stabilizing abilities of hydrophobic components. [10, 11]

In the following work, the synthesis routes of different amphiphilic block-copolymers using ring-opening polymerization (ROP) with the low toxicity organic based catalyst 1,8-diazabicyclo[5.4.0]undec-7-ene (DBU) are employed. Furthermore, free radical

polymerization of acrylic acid-based polymers is described and discussed to form pH-responsive polymeric NPs through FNP. The polymers are extensively characterized with respect to their structural by nuclear magnetic resonance (NMR) and thermal properties by thermogravimetric analysis (TGA). The polymers are used to form bare polymeric nanoparticles using the MIVM FNP setup. Novel experiments combining the amphiphilic block-copolymers with oleic acid-coated IONPs are presented to understand the mechanism and interaction between the two material groups during NPs synthesis in the MIVM FNP setup.

2. Background and literature review

2.1 Polymers in NPs for drug delivery

About 70-90 % of newly developed drugs have a low water solubility and cannot be administered into the human body directly [12]. The addition of hydrophilic polymers to the drugs can increase solubility and help to reduce immunogenicity and toxicity of the particle. A hydrophilic polymeric coat might also allow for an increase in the bioavailability of these drugs and enable oral or intravenous uptake [13]. Furthermore, the coating allows for side specific drug release through targeting ligands added to the polymeric shell. The drug of interest can be either covalently linked to the polymer by grafting the polymer onto the drug´s surface, or it can be encapsulated inside a liposome or polymersome or associated within a polymer matrix (bicontinuous nanospheres or hydrogel). The formation of a specific size and type of these self-assembled NPs is highly dependent on the process parameters and the type of polymer used [14, 15]. Since the polymers function as drug delivery vehicles, only polymers can be used that are approved by the regulatory authorities such as the Food and Drug Administration (FDA) or the European Medicines Agency (EMA). The polymer should be readily biodegradable and should not leave any toxic residues in the body behind. [13, 16]

2.1.1 Types of polymers for NPs synthesis

For the synthesis of NPs all types of polymers can be used. Linear polymers are macromolecules, that have one continuous backbone with each repeating unit only connected to two other units. The simplest linear polymer is a ***homopolymer*** made up of only one type of monomer. Complex homopolymers like poly(2-(2-ethoxyethoxy)ethyl acrylate) (PEEA) with a repeating unit that consists of a hydrophilic and hydrophobic part can self-assemble and form stable NPs [17]. Linear polymers with more than on type of repeating monomer unit are ***copolymers***. The three different types of copolymers are alternating-, random- and block-copolymers (Figure 2). In drug delivery applications the main type of polymer used is a block-copolymer made up of two or more uninterrupted blocks of repeating units. Dependent on the number of blocks, a diblock, triblock or multiblock block-copolymer can be synthesized. Compared to the alternating- and random-copolymer, the domains of the block-copolymer chain can have different physico-chemical properties. Variations in the solubility of the blocks (e.g., one being hydrophilic, the other more hydrophobic) lead to higher affinity of certain domains and the possibility to self-assembly into NPs [13]. Poly(ethylene glycol)-*b*-poly(lactic-co-glycolic acid) (PEG-PLGA) is a common example for such amphiphilic diblock block-copolymer [18]. Another type of polymer are ***branched copolymers***. Instead of a single continuous backbone, they consist of branches to form comb-, star- or hyperbranched-polymers. Different repeating units can enable the

formation of branches to ultimately form large polymer structures. In drug delivery applications branched polymer structures show high drug loading and controllable drug release mechanism by changing structural properties [19]. An overview of the different polymer types is presented below (Figure 2). [20]

Common characterization methods to identify the polymer structure include NMR, Fourier-transform infrared spectroscopy (FTIR) and gel permeation chromatography (GPC). Thermal properties can be determined by TGA and differential scanning calorimetry (DSC). Molecular weight determination and calculation of degree of polymerization (DP) helps to define the polymer's structure. The dispersity ($Đ_m$) is calculated by the ratio of weight average molecular weight (M_w) over the number average molecular weight (M_n) and measures the width of the chain lengths distribution that are present in a sample (Equation (1)).

$$Đ_m = \frac{M_w}{M_n} \tag{1}$$

In polymer synthesis a low $Đ_m < 1.2$ indicates a controlled polymerization with similar chain length distribution. For commercial polymers the $Đ_m$ of the reaction ranges from 1.5 to 2.5, followed by separation into different molecular masses by GPC. The nomenclature of a block copolymer consisting of PEG ($M_n = 5000$ g/mol) and PLGA (lactic acid (LA) $M_n = 7500$ g/mol; glycolic acid (GA) $M_n = 2500$ g/mol) is written as PEG_{5K}-$PL_{7.5K}G_{2.5K}A$. [20]

2.1.2 Types of self-assembled polymeric NPs

The previously introduced polymers can be used to form different types of polymeric nanoparticles (Figure 2). Copolymers can self-assemble in aqueous solution into ***core-shell polymeric micelles*** by the interactions of the hydrophobic core. The hydrophilic domains shield the core from unfavorable interactions with water. Using a homopolymer in combination with a stabilizer similar NPs can be formed through methods like (flash) nanoprecipitation. Hydrophobic drugs can be present in the hydrophobic domain increasing the solubility and bioavailability [21]. ***Polymersomes*** are polymeric NPs like liposomes with a hydrophobic circular domain, shielded from both sites with hydrophilic polymers. Commonly diblock- and triblock-copolymers are used for the formation of the polymersomes. When compared to polymer micelles additional hydrophilic drugs can be loaded into the hydrophilic core of the polymersomes [22]. Solvent emulsification or solvent displacement methods, like (flash) nanoprecipitation are used for the fabrication of polymersomes [15]. ***Bicontinuous nanospheres*** are polymeric nanoparticles with an outer hydrophilic domain and a core with a mixture of hydrophilic and hydrophobic domains. This allows for versatile drug loading of hydrophilic and/or hydrophobic molecules. Similar to polymersomes tuning the process parameters of the solvent emulsification or solvent displacement methods results in bicontinuous nanospheres [23]. Other possible types of self-assembled NPs are

dendron micelles, consisting of linear-dendron block-copolymers, or ***janus dendrimers*** with hydrophilic and hydrophobic domains. Both structures are made from dendritic molecules providing superior shielding of hydrophobic domains compared to linear copolymers. Hydrophobic drug loading has also been proven successful [24]. By changing types of polymers and optimizing process parameters polymeric NPs can be designed to hold hydrophilic or hydrophobic drugs and allow for increased bioavailability. [13, 25]

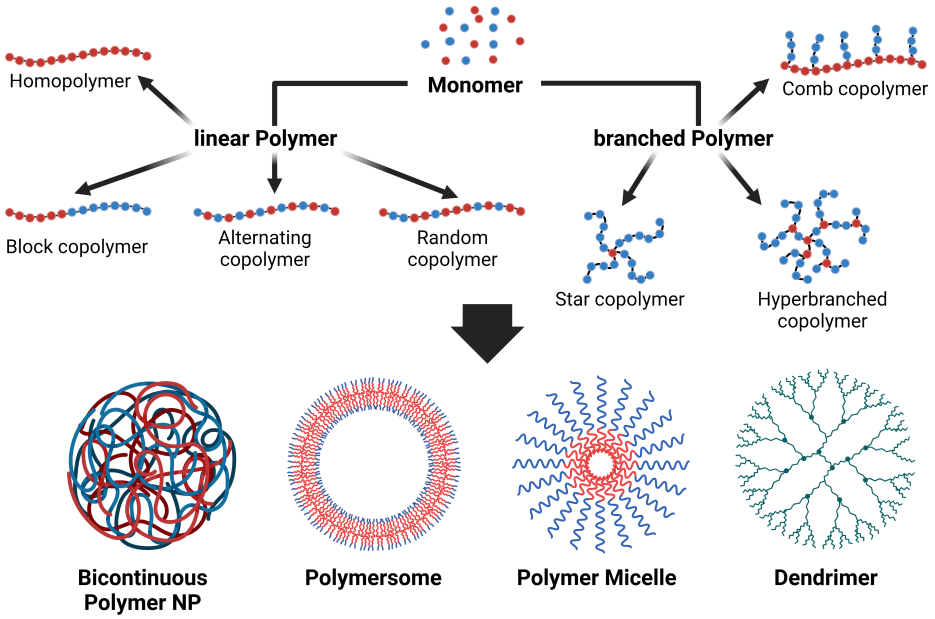

Figure 2: Types of different copolymers and formation of (self-assembled) polymeric Nanoparticles.

2.1.3 Approved (co)polymers in biomedical application

Until now three groups of polymers have been approved for drug delivery applications the FDA. One application being the encapsulation of drugs by liposomes with low molecular weight PEG as hydrophilic domain mainly serve to increase the bioavailability of certain cancer drugs and decrease their toxicity. In another drug delivery systems, the drugs are embedded in PEG-PLGA matrixes for prolonged drug circulation times. Most commonly pegylated proteins are used for overall improved protein stability in various drug applications. Consequently, PEGylation increases the half-life of the proteins and thereby helps to reduce significantly the amount of drug to be administered. PEGylation of liposomes was also used to increase the stability of the mRNA vaccines produced by Moderna or BioNTech/Pfizer during the COVID-19 pandemic. [26, 27]

Since more than 70% of newly developed drugs show low (aqueous) solubility and require modifications to increase bioavailability, further investigation in the formation of polymeric NPs is required [12]. The need for high volume fabrication of NPs is increasing and cheap and scalable methods like FNP will gain in importance.

2.2 Flash nanoprecipitation for polymeric NP formation

Various methods have been established for the fabrication of polymeric nanoparticles. There are two distinct pathways for the formation of polymeric nanoparticles. ***Direct methods*** include polymerization to form NPs through anionic emulsion polymerization or the synthesis of large dendritic structures. ***Indirect methods*** use diffusion of dissolved preformed polymers into an antisolvent to form NPs. Examples are the self-assembly of amphiphilic block-copolymers into micelles or polymersomes. Other methods include the emulsification-diffusion method (formation of NPs from an emulsion) and the solvent displacement method (nanoprecipitation and flash nanoprecipitation). The solvent displacement methods, especially the FNP, allow for fast one step homogeneous NPs synthesis. Furthermore, the process allows ease of drug addition compared to indirect methods. [24, 25, 28]

2.2.1 Concept of Flash Nanoprecipitation

The ***solvent displacement method*** is a simple one step manufacturing process of NPs. A water miscible organic solvent is used as the polymer solvent. Common organic solvents are dimethylsulfoxide (DMSO), tetrahydrofuran (THF), methanol or acetone. The organic solvent containing the polymer is injected into the antisolvent (Water), where the polymer precipitates. The conventional method of solvent displacement includes the method of nanoprecipitation, where droplets of the organic solvent is injected into a vial containing the stirring antisolvent in bulk. The setup does not require any specific reactor and formations of a wide range of polymeric nanoparticles can be performed. A significant drawback of the traditional nanoprecipitation method is the lack of control during mixing (use of a stirring bar for mixing) as well as the resulting wide particle size distribution. [21, 29, 30]

Flash nanoprecipitation (FNP) first developed by Brian K. Johnson and Robert K. Prud'homme addresses these issue by the addition of a mixing chamber for the polymer-containing solvent and the anti-solvent [11]. The core mechanism that is used is the injection of the solvent and anti-solvent through two or more-inlets into a special reactor at high speeds and a short mixing interval of milliseconds. Syringe pumps are used to move the two streams at desired rates towards the reactor. The two types of reactors currently in use are the multi-inlet vortex mixer (MIVM) [31] and the confined impinging jet (CIJ) [11] (Figure 3) [11, 31, 32]. The major difference between the two geometry types is the possible ratio between the two mixing solutions. The CIJ is limited to two inlets with equal flow rates. The MIVM is well scalable and can surpass the pump limitations by adding inlets to the design as well as by varying the solvent/anti-solvent ratio. Inside the reactor rapid turbulent mixing occurs resulting in local supersaturation and the formation of polymer nanoparticles. The formation is kinetically controlled and parameters like flow rates and solvent/anti-solvent

ratios directly influence the resulting NPs sizes. For biomedical applications additional components, such as anti-cancer drugs and fluorescent polymers, can be added to the solvent or anti-solvent. These components can be added to the coating or encapsulated inside to form multifunctional polymer NPs. The product is removed from the reactor by one outlet. This process can also be easily scaled up to industrial size for synthesis of large quantities of Nanoparticles. [21, 32]

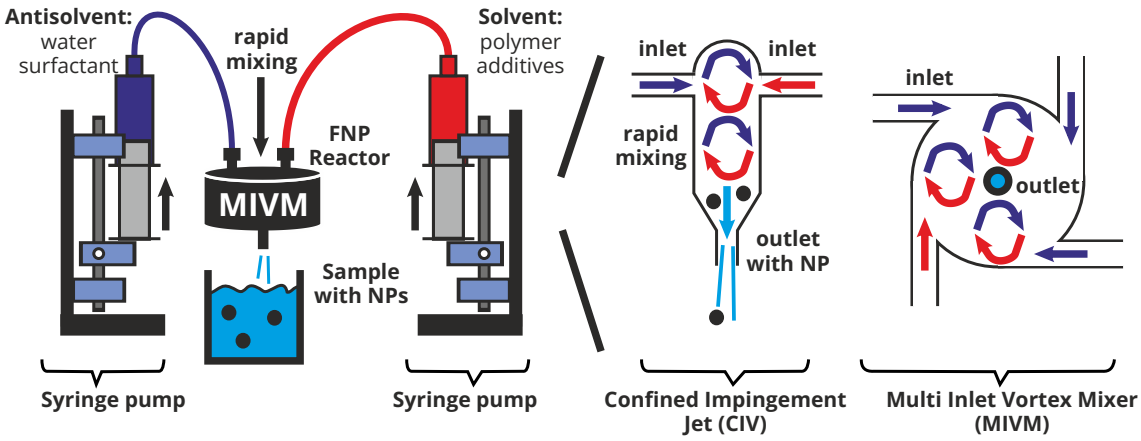

Figure 3: Flash nanoprecipitation setup and common reactor types (confined impingement jet (CIJ) and multi inlet vortex mixer (MIVM).

2.2.2 Nucleation and growth theory of particle formation in FNP

Supersaturation (S) is described by the solute concentration (C) divided by the equilibrium solubility concentration (C^*) (Equation (2)). A solute concentration above the nucleation concentration (C_{min}) results in the self-assembly and formation of new nuclei. The formation of nuclei leads to a decrease in the solute concentration and the growth mechanism by diffusion to already formed particles is facilitated. Below C_{min} the solution does not form new particles and growth and aggregation of already formed particles is the primary mechanism. When the solute concentration equals the equilibrium solubility concentration, growth of the particle by solute addition is stopped. The formed NPs can be stabilized in solution by addition of stabilizing agents. [33]

$$S = \frac{C}{C^*} \tag{2}$$

In the flash nanoprecipitation process the formation of the polymeric NPs can be explained by the La Mer mechanism. The organic solvent containing the polymer solute meets an anti-solvent at very high speeds in a confined reactor (Stage I) (Figure 4) [10, 21, 34]. Both streams mix turbulently in a short period of few milliseconds. The polymer and hydrophobic solutes from the organic phase directly enter a supersaturated concentration in the antisolvent close

to the critical limiting supersaturation (C_{max}) (Stage II). High number of monodisperse nuclei are formed, and solute concentration decreases rapidly. The particles grow by the interaction of the remaining hydrophobic solutes with the nearby formed nuclei (Stage III). To achieve monodisperse particles, the induction time for the nucleation and growth ($t_{nuc,gro}$) needs to be longer than the mixing time of the two miscible solvents (t_{mix}). This allows nucleation to dominate the process. In this case the diffusion-limited growth does not define the particle size. Similarly, the induction time for the diffusion-limited aggregation of the particles need to be longer (t_{agg}) than the mixing time to avoid a significant particle size increase and particle polydispersity. Size, number-density, and polymer-polymer interaction define the actual aggregation behavior. Cluster-cluster aggregation can be controlled by stabilizing the formed NPs. After this point, the equilibrium solubility of the solvent/anti-solvent mix is reached and the particle size stays constant as long as the nanoparticles are stabilized by an amphiphilic layer from a surfactant or block copolymer. [10, 21, 34]

To understand further the nucleation during FNP, the nucleation rate (J) can be used (Equation (3)). In FNP, a high rate of nucleation is preferred to yield a monodisperse distribution of NPs. The nucleation rate is directly dependent on the temperature (T), surface tension (γ), molar volume (v), Boltzmann constant (k) and supersaturation (S). When increasing the supersaturation, the rate of nucleation increases facilitating the formation of higher number of monodisperse nuclei. Change in mixing time and solute concentration have significant effect on the resulting polymer NPs properties. [10, 21, 33]

$$J = A * exp\left(\frac{-16\pi\gamma^3 v^2}{3k^3T^3(ln(S))^2}\right) \tag{3}$$

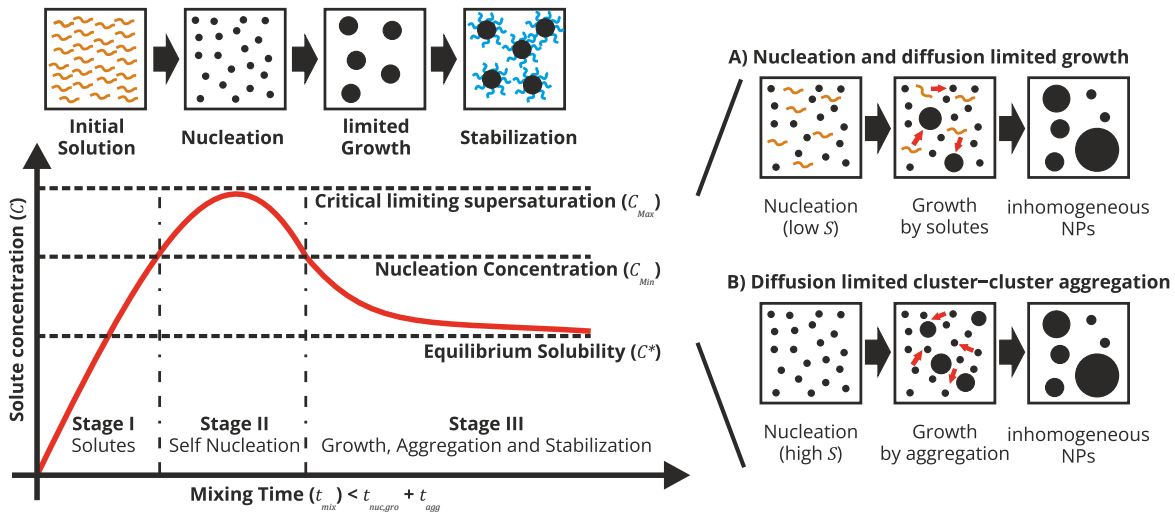

Figure 4: La Mer Diagram: formation of NPs through Supersaturation (S) in FNP reactor.

2.2.3 Polymer particle stabilization

In FNP the formation of polymeric NPs is kinetically controlled. Hydrophobic interaction between the NPs occur and the stability of the formed NPs are low. The stabilization and prevention of aggregation can be achieved by two different methods.

The hydrophilic part (e.g., PEG) of the amphiphilic block-copolymer can associate with the water molecule and lead to stable core-shell structures. In this case the PEG stabilizes and shields the hydrophobic core from unfavorable interaction with water and prevents growth. [18, 35]

Additional stabilizing agents in form of amphiphilic structures can be added to the anti-solvent to prevent the hydrophobic polymer and drug structure to aggregate and precipitate. During the formation of the particles in FNP, the hydrophobic part of the stabilizer of the amphiphilic stabilizer associates with the hydrophobic polymeric NPs structure and shields it from unfavorable interaction with the water molecules. At the same time this mechanism also impedes any further growth of the particles. Common NPs stabilizers for FNP are PVP or polysorbates. Added stabilizers should be approved biocompatible molecules. [32]

2.2.4 Parameters influencing the FNP process

The size and size distribution of the resulting polymeric NPs can be controlled by varying either the kinetic parameters of the particle formation or the rate of nucleation (Equation (3)). Traditional growth and nucleation mechanisms by dissolved polymer addition do not play a significant role in the formation of the NPs through FNP [21]. Kinetic parameters do have a more important role.

Polymer Concentration:

The polymer concentration in the solvent significantly influences the size of the resulting polymeric NPs. With a higher polymer concentration, the supersaturation is increased and nucleation rate increases (Equation (3)). The number of nuclei in the sample is increased, leading to more interaction between the polymers. This results in particle size enlargement [21]. FNP systems with purely hydrophobic polymers or drugs require amphiphilic polymers or stabilizing agents to halt the aggregation of these components. Increasing the concentration of the stabilizing agent prevents further growth by aggregation and reduces the particle size. [32]

Molecular weight:

The molecular weight of an amphiphilic block-copolymer does not significantly affect the size of the formed polymer NPs [2]. However, by adding hydrophobic molecules with higher molecular weight an increase in the size of resulting particles is observed. Changes in the

supersaturation, the number of nuclei formed as well as in the interaction between the polymers contribute to the increase [32, 34].

Flow Rate/Solvent to Antisolvent Ratio:

The influence of the flow rate on the size of the resulting nanoparticles are directly related to the Reynolds number (Re). An approximate definition of Re for the MIVM is given below (Equation (4)). For each inlet (i) the Re is calculated by the volumetric flow rate (V_i) multiplied by the diameter of the reactor (L) and divided by the kinematic viscosity (v_i) of the corresponding stream. Kinematic stream viscosity is defined by the viscosity (η_i) of the liquid divided by the density (p). [36]

$$Re = \sum_{i=1/N} \frac{V_i * L}{v_i} \qquad v_i = \frac{\eta_i}{p_i} \tag{4}$$

An increase in Re leads to higher flow rates and turbulences inside the reactor creating higher local supersaturation. The particle size decreases. At a Re above >2000 the turbulences inside the reactor are maximized. Further increase in supersaturation is not possible, limiting the minimum particle size for this geometry. Decreasing the ratio of solvent to anti-solvent at the same Re induces higher supersaturation and reduces the particle size. [36]

Type of Polymer:

In flash nanoprecipitation the type of polymer directly influences the supersaturation in the reactor. Polymers can have different solubility dependent on their chemical structure. The solubility can be expressed by molecular models like the Hildebrand solubility parameter (δ_{HiSP}), Hansen solubility parameter (HSP) [37] or Hoy solubility parameter (δ_{Hoy}) [38]. The latter two use three different parameters for dispersion (δ_D), polar (δ_P) and hydrogen (δ_H) interactions to accurately define the overall solubility of a polymer (Equation (5)). [2, 35]

$$\delta_{HiSP}{}^2 = \delta_D{}^2 + \delta_P{}^2 + \delta_H{}^2 \tag{5}$$

Decreasing the overall solubility of the polymer in the antisolvent increases the supersaturation and reduces the particle size. In the case of block-copolymers, the solubility of each polymer block needs to be considered separately. Similar solubility parameters cause the hydrophilic domain to be entrapped in the core reducing the shielding of hydrophobic core and decreasing the stability of the nanoparticle. Ostwald ripening caused by diffusion of entrapped hydrophilic domains to the surface of the particles, leads to dissolution and addition of polymer to form larger particles. Thermal properties of the polymer can also affect the ability to form stable particles. Low melting (T_m) and/or glass transition temperature (T_g) can lead to high polymer mobility in the core of the NPs and aggregation of particles. [2, 35]

Solvent

By using different solvents the solubility of the polymer changes, affecting the supersaturation conditions in the reactor. Some solvents show higher diffusion compared to others. Increase in Ostwald ripening can be observed reducing the stability of the NPs. Possible removal of the organic solvent is vacuum evaporation or dialysis. [10, 35]

For characterization of the resulting NPs size measurements are performed by dynamic light scattering (DLS) and (scanning) transmission electron microscopy (STEM). Using special gold electrodes, DLS also enables the measurement of the Zeta potential giving information on the stabilization of the NPs.

2.3 Amphiphilic Polymer synthesis

Copolymerization is necessary to form amphiphilic polymers that can be used for the stabilization and formation of NPs in FNP. A-B block copolymers (Figure 2) are the most prevalent types of polymers used for these applications. These are synthesized by sequential polymerization of the two blocks through chain-growth polymerization. To yield a diblock copolymer, monofunctional initiators are used for the reaction. Both free radical and ionic polymerization are common methods for the synthesis of block copolymers. In the application of FNP polymers like poly(ethylene glycol)-*b*-poly(lactic acid) (PEG-PLA), PEG-PLGA [2] and poly(acrylic acid)-*b*-poly(styrene) (PAA-PS) [39] have been demonstrated to yield polymeric NPs (Table 1). Discussed below is the anionic ring-opening polymerization (ROP) of hydrophobic cyclic esters from a hydroxyl functionalized hydrophilic macroinitiator. [20, 40, 41]

2.3.1 mPEG-OH synthesis

ROP macroinitiator methoxy poly(ethylene glycol) (mPEG) to form the hydrophilic block of the copolymer is commonly used for the synthesis of amphiphilic copolymers. Depending on the functionalization of the PEG diblock (mPEG) or triblock copolymers (PEG) can be polymerized. PEG, is biodegradable, biocompatible as well as approved by the FDA for drug formulations [42]. Besides multiple approved PEG-containing macromolecular drugs, two FDA and EMA commercially approved NPs pegylated liposomes containing doxorubicin (Caelyx®) [43] and irinotecan hydrochloride trihydrate (Onivyde®) [44] show the possibility of NPs in cancer treatment. Another possible future application includes poly(ethylene glycol)-*b*-poly(caprolactone) (PCL-PEG) for controlled insulin delivery [45]. PEG stabilizes the nanoparticle surface and allows it to prevail longer in the human body by preventing adsorption to proteins [16, 42]. Monofunctional mPEG is synthesized commercially by anionic polymerization with methanol as the initiator and ethylene glycol or ethylene oxide as the monomers. Molecular weights of 500 g/mol up to 20000 g/mol for pharmaceutical applications are widely available. [46, 47]

2.3.2 PAA-OH synthesis

Another macroinitiator for the ROP of cyclic esters is hydroxyl-terminated poly(acrylic acid) (PAA-OH). The carboxyl group enables the polymer to be pH-responsive by enabling ionic interactions with surrounding molecules. PAA is nontoxic and biocompatible. The free radical polymerization of PAA-OH is done in an organic solvent (THF) together with the initiator azobis(isobutyronitril) (AIBN) at 65 °C under argon gas (Figure 5) [48]. The functionalization of hydroxyl group is achieved by the addition of 2-mercaptoethanol (ME) through

telomerization with the acrylic acid. The ME acts as a chain transfer agent and regulator for the molecular weight during the reaction. Successful synthesis of PAA-OH was reported for 1200 g/mol and 7300 g/mol PAA-OH. [20, 48–50]

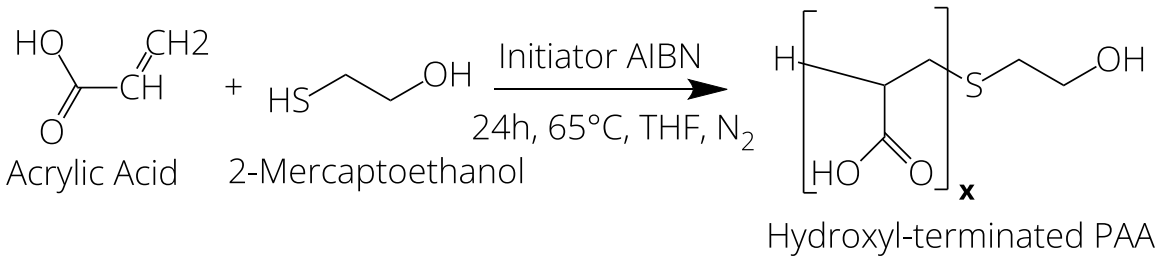

Figure 5: Free radical polymerization of hydroxyl terminated PAA.

2.3.3 $Sn(Oct)_2$ catalyzed synthesis of PLGA

Stannous octoate ($Sn(Oct)_2$) represents the most common catalyst for the bulk synthesis of PLA, PLGA and PCL for industrial and research application. This catalyst is also used for the polymerization of the commercially available PLGA, with exception of some low molecular weight PLGA produced by direct polycondensations (Evonik) [51]. The two main disadvantages of this catalyst are the high temperature of 120 °C-180 °C needed to polymerize an equal ratio of PLGA with a low polydispersity and the increased toxicology of the product introduced by the tin. This limits the usage of the catalyst in biomedical application. [52]

The catalyst is using hydroxyl groups as macro initiators, while carboxylic groups do not initiate the reaction. Water should be removed from the reaction, because a protic agent can act as co-initiator or promote chain transfer [53]. The amount of initiator determines the molecular weight of the resulting polymer. $Sn(Oct)_2$ reacts with the hydroxyl group of the macroinitiator to form a tin alkoxide complex. The polymerization proceeds by the coordination–insertion mechanism of the monomer units glycolide or lactide for PLGA. Random copolymerization of lactide and glycolide has been a challenge, because of the difference in reactivity ratio of 14 : 1 favoring glycolide. Throughout the polymerization the amount of lactide in the chain increases with lower concentration of free glycolide monomers in the bulk. [50, 52, 54, 55]

PAA-OH [48, 50] as well as mPEG-OH [56] are successfully polymerized with glycolide and lactide for the formation of amphiphilic block-copolymers PAA-PLGA and PEG-PLGA. The molecular weight of the polymers can be larger than 200,000 g/mol [57].

2.3.4 DBU catalyzed synthesis of PLGA

Metal free catalysts offer another relatively new reaction pathway for the synthesis of PLGA and other cyclic esters. Compared to the previously described tin containing metal complexes, organocatalytic reactions inherently show a lower toxicity. The separation of the catalyst from the polymer is efficient [58].

The organic catalyst DBU is used for the fabrication of cyclic esters (PLA/PLGA/PCL) from a halide solution at room temperature. The amidine group functions as a strong base and initiates the ROP. Similar to the $Sn(Oct)_2$ catalyst, DBU starts the polymerization by reacting with an macroinitiator composed of an hydroxyl group. The initiator mPEG is synthesized with D,L-lactide and glycolide forming the amphiphilic block-copolymer mPEG-PLGA (Figure 6). In batch polymerization the higher reactivity rate of glycolide results in the formation of a gradient copolymer. As large blocks of glycolide show low solubility in most organic solvents, a semi batch polymerization has been proposed by Qian et al. [59]. glycolide is added continuously to the solution containing the macroinitiator, LA and DBU resulting in a nearly random copolymer of PLGA. [40, 59, 60]

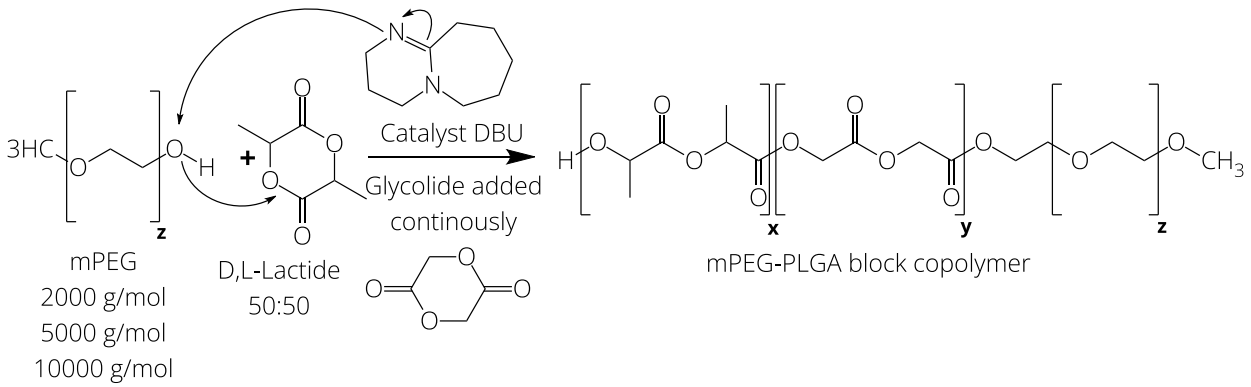

Figure 6: Semi-batch DBU-catalyzed ring opening polymerization of PLGA by the macroinitiator mPEG.

The polymerization can be initiated by two different mechanisms, the activated ***alcohol pathway (AAP)*** or the ***nucleophilic attack pathway (NAP)*** (Figure 7). In the presence of an excess of hydroxyl groups, the polymerization proceeds by the AAP reaction. The DBU amide group attacks the proton from the hydroxyl group forming a hydrogen bond complex between the mPEG and DBU. The ROP is initiated by the negative charge on the oxygen attacking the polarized carbonyl group of the cyclic ester LA or GA. The polymer chain is propagating by “quasi” anionic cyclic ester addition behaving as a living polymerization. In absence of the hydroxyl bonds, the polymerization proceeds as NAP. The amide group of the DPU directly attacks the polarized carbonyl group of the cyclic ester LA or GA. The monomer is covalently bound to the initiating DBU, while another DBU molecule proceeds with the

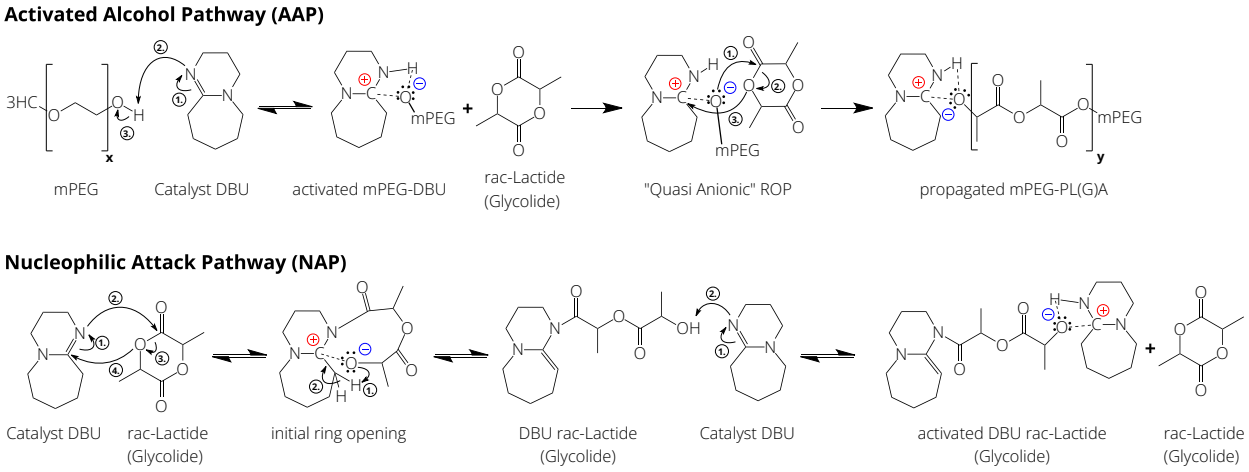

Figure 7: Different activation reaction pathways for DBU-initiated ROP polymerization.

propagation of the chain from the hydroxyl group. The polymerization proceeds with a "quasi" anionic cyclic ester addition. [40, 60]

The reaction kinetics for a low temperature ring opening polymerization catalyzed by DBU for LA and GA are explained through following equations (Equation: (6)) [59, 61]. The reaction rate constant (k) depends on the three concentrations of monomer LA/GA, catalyst DBU and propagating mPEG as macroinitiator. These concentrations describe the concentration change of monomer LA/GA over time. The first order rate constant difference between GA and LA is reported as 10^3. GA lacks the methyl group compared to LA resulting in a higher area of attack and lower steric hindrance for the catalyst DBU. [59]

$$\frac{d[monomer]}{dt} = -k * [catalyst] * [propagating\ chain] * [monomer] \qquad (6)$$

Lohmeijer et. al. proposed that the reaction kinetics for the ROP follows a first-rate reaction order as described here (Equation (7)). The apparent rate constant (k_{app}) follows a linear slope for a fixed amount of catalyst and macroinitiator. This case assumes that changing the amount of DBU to propagating mPEG follows the same reaction pathway of only AAP and/or NAP at all times. [59, 61]

$$k_{app} = -k * [catalyst] * [propagating\ chain] \qquad (7)$$

Sherck et al. presented that the apparent rate constant in a DBU, mPEG and LA system is only constant for low conversion and/or low molar ratio of catalyst to mPEG (< 1 : 1) [40]. In excess of catalyst the reaction follows the NAP pathway, forming ketene aminal groups. Besides the NAP and AAP pathway the reaction also shows the ***acylation pathway*** (Figure 8), increasing the dispersity of the polymers $Đ_m$ by recombination of propagating chains. At this point the reaction does not show a living behavior. The reaction rate is not constant, following extensive kinetic systems. [40, 60]

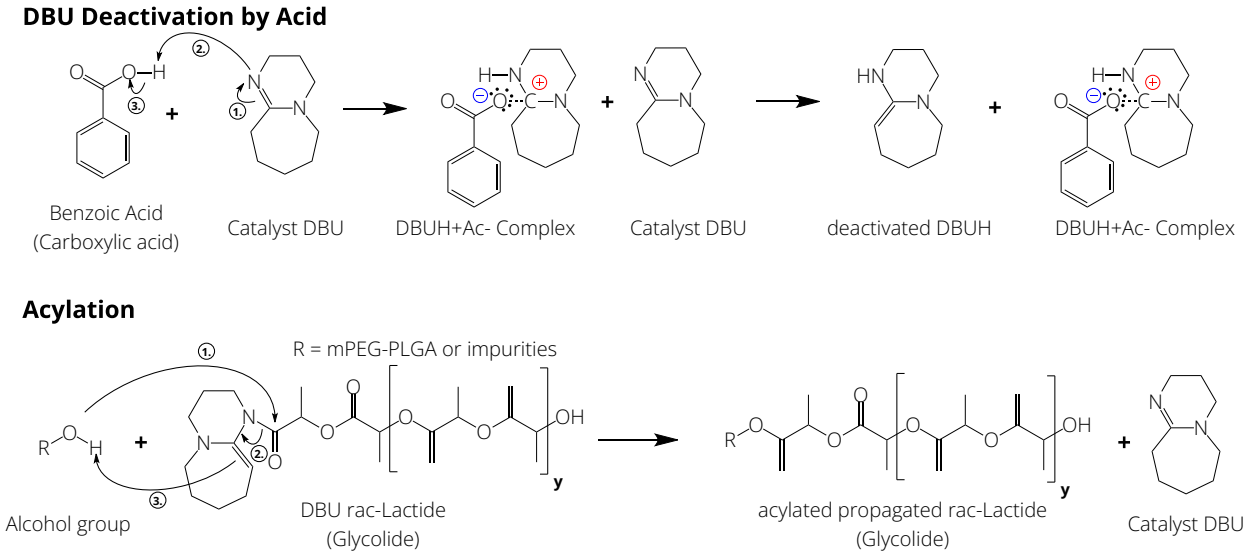

Figure 8: Deactivation of DBU through addition of carboxylic groups; Acylation process in access DBU following the NAP pathway.

The ROP is terminated by the ***addition of a carboxylic group*** in form of an acid (Figure 8). Commonly benzoic acid or acrylic acid is used. The amide group of the DBU is protonated through a nucleophilic attack towards the carboxyl acid group. This causes the formation of a carboxylic acid DBU-complex. In presence of further unprotonated DBU-amide groups, the methylene group is deprotonated and the complex between the initial DBU and the acid group is dissolved. This reaction proceeds until every catalyst molecule is deactivated. [40, 60]

To further understand the structure of the polymers during and after the ROP, the sequence length of the glycolyl ($\overline{L_{GA}}$) and lactyl ($\overline{L_{LA}}$) repeating units can be determined by C13 NMR. The block length of GA and LA directly influence resulting properties like solubility. Depending on the carbon of the next repeating unit (methine for lactide, methylene for glycolide) different resonance shifts of the carbonyl carbons can be observed. By comparing the integrals of the two carbons the average sequence length of the lactide and glycolide blocks can be determined with following equations (Equation (8)(9)). [59, 62, 63]

$$sequence\ length\ \overline{L_{LA}} = \frac{I_{LL}}{I_{LG}} + 1 \tag{8}$$

$$sequence\ length\ \overline{L_{GA}} = \frac{I_{GG}}{I_{GL}} + 1 \tag{9}$$

The sequence length of GA is of special importance as an average $\overline{L_{GA}}$ of 4 or higher results in insolubility of the polymer in solvents like THF and dichloromethane (DCM). Previous experiments from the specialization project have shown that a semi-batch polymerization with LA:GA ratio of 50 : 50 did result in early precipitation and insolubility of the polymer PEG-PLGA. [59, 64]

2.3.5 DBU catalyzed synthesis of PCL

ε-caprolactone (CL) has been extensively studied to polymerize through anionic ROP to PCL with $Sn(Oct)_2$ as a catalyst. The toxicity of $Sn(Oct)_2$ and residual tin limits the use in biomedical applications and requires extensive cleaning procedures [65]. Lohmeijer et. al. has demonstrated the use of organocatalysts for the synthesis of PCL at room temperature. A combination of DBU and a co-catalyst containing a thiourea group results in high conversion of CL. Without a co-catalyst containing a thiourea group polymerization is not possible at room temperature (RT), because of low reaction rates. [61]

The cocatalyst containing thiourea groups are not easily available. Polymerization at elevated temperatures of 80-100 °C and increased pressure enables the direct polymerization of CL to PCL with only DBU as a catalyst (Figure 9). The reaction requires total absence of oxygen to inhibit early degradation and DBU deactivation by oxidization. Copolymerization of CL with $mPEG_{2K}$ at a temperature of 90 °C yields a conversion of over 90 % as presented by Chen et al. [41]. The molecular weight corresponds to the expected value and an excellent $Đ_m$ of 1.15 was achieved for PEG_{2K}-$PCL_{5.3K}$. At 90 °C the reaction rate for the polymerization was fast enough to yield good conversion, while the degradation rate of the DBU was still low. Using only DBU as an catalyst for PEG-PCL polymerization is a promising alternative to the established $Sn(Oct)_2$ method. [41, 66]

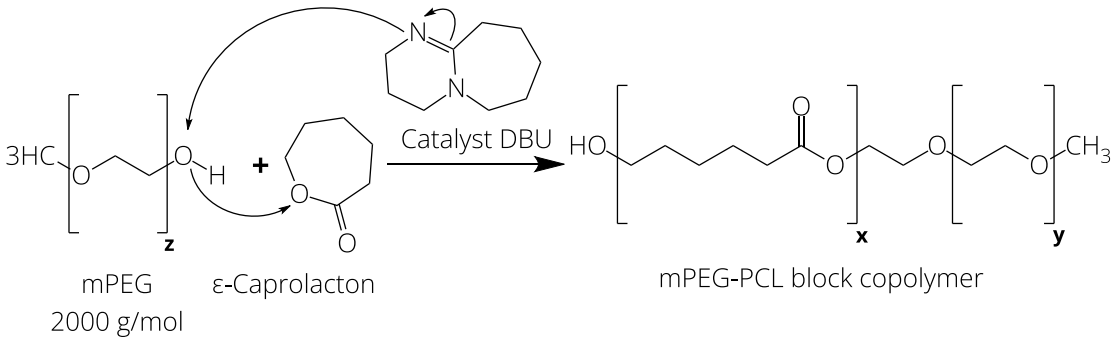

Figure 9: Synthesis of PEG-PCL block-copolymer using DBU as catalyst at elevated temperatures 80-100 °C.

2.4 Block-copolymer systems in FNP

Previously, many block-copolymers have been tested in the flash nanoprecipitation process. The most used biocompatible compounds are based on the hydrophilic part PEG and hydrophobic PLGA. Zhu et. al. [2] and Pustulka et. al. [35] have tested different amphiphilic block-copolymers in regards of their particle size formation and stability of the NPs for the model drug β-carotene in the FNP system using a MIVM (Table 1). The researchers revealed that the stability of the particles directly relate to material properties of the hydrophobic and hydrophilic part. The solubility difference of the two domains should be high enough, the glass transition temperature should be above 37°C and the Re should be above 3000 to guarantee stable monodisperse NPs through the MIVM process. The research also revealed that incorporation of hydrophobic drugs is only possible for a certain hydrophilicity range. Highly hydrophobic particles result in instability of the NPs and fast Ostwald ripening. [2, 35]

Markwalter et. al. [39] used PAA-PS block-copolymers to form stable NPs around the drug dextran through the low volume µMIVM. In this case chloroform ($CHCl_3$) was used as an antisolvent compared to water in traditional cases. The researchers showed that stable NPs could be formed in this way. [39]

Table 1: Common block copolymers for FNP NPs formation with sizes and drugs used.

Polymer	Nanoparticle size (nm)	Solvent	Drug	Reactor Type	Ref.
PEG-PLA	20-41	THF : H_2O	β-carotene	MIVM	[2, 35]
PEG-PLGA	34-69	THF : H_2O	β-carotene	MIVM	[2, 35]
PEG-PCL	42-147	THF : H_2O	β-carotene	MIVM	[2, 35]
PEG-PS	25-36	THF : H_2O	β-carotene	MIVM	[2, 35]
PAA-PS	75-80	H_2O : $CHCl_3$	dextran	µMIVM	[39]
PEG-PSS	~50	THF : H_2O	OA IONPs	CJI	[67]
PEG-PLA	115	THF : H_2O	OA IONPs	CJI	[1]

The encapsulation of hydrophobic oleic acid (OA) coated IONPs has been successfully studied by Modak et. al. [67] using the poly(ethylene glycol)-*b*-poly(propylene sulfide) (PEG-PSS) and Fuller et. al. [1] using $PEG_{4.9K}$-PLA_{6K} amphiphilic block-copolymers. For both coating processes of OA IONPs the CIJ reactor geometry was used. Both researchers were able to embed multiple OA IONPs into a single polymeric NPs (Table 1). Sizes of under 150 nm were achieved, but samples showed high degree of polydispersity. [1, 67]

In this work the polymerization of different block-copolymers is combined with the addition of the hydrophobic OA coated IONPs in the MIVM geometry during FNP. Compared to the literature presented above, the MIVM should allow for better control of the process parameters and therefore result in lower polydispersity of the polymer OA IONPs system.

3. Materials and methods

3.1 Materials and general procedures

A List of all Chemicals used for the polymer synthesis and nanoparticle formation is listed below (Table 2). If not otherwise specified, the chemicals were used as they are.

Table 2: List of Chemicals used in Experiments.

Chemical	CAS number	Product number	Molar mass M (g/mol)	Remarks
2-propanol	67-63-0	20922	60.2	technical
Acetone	67-64-1	20063	58.08	technical
AIBN	78-67-1	714887	164.21	0.2M solution Toluene
Benzoic acid	65-85-0	8.22257	122.12	-
Chloroform	67-66-3	1.02445	119.38	analytical; water < 0.01 %
Chloroform-*d*	865-49-6	151823	120.38	NMR solvent
DBU	6674-22-2	8.03282	152.24	-
DCM	75-09-2	494453	84.93	anhydrous; water < 0.002 %
DMSO-*d6*	2206-27-1	1.03424	84.17	NMR solvent
Diethyl ether	60-29-7	296082	74.12	anhydrous
ε-Caprolactone	502-44-3	17344250	114.14	-
Ethanol	64-17-5	83804	46.07	technical
Glycolide	502-97-6	G1796	116.07	hydrolysis ready, freezer
Magnesium SO_4	7487-88-9	208094	120.37	anhydrous, reagent
ME	60-24-2	M6250	78.13	
MQ-water	-	-	18.02	MQ-water dispenser
$mPEG_{2K}$	9004-74-4	202509	2000**	-
$mPEG_{5K}$	9004-74-4	81323	5000**	-
$mPEG_{10K}$	9004-74-4	732621	10000**	-
PLGA RG503H®	26780-50-7	719870	22471***	-
rac-Lactide	95-96-5	303143	144.12	hydrolysis ready, fridge
$Sn(Oct)_2$	301-10-0	S3252	405.122	-
THF	109-99-9	1.08101	72.11	analytical; water < 0.02 %
	109-99-9	401757	72.11	
Tween80®	9005-65-6	P1754	1310	-

*All SDS and Specification Sheets can be found here
**Confirmed by NMR Analysis (6.3 NMR spectra of PEG-PL(G)A samples)
***M_n Calculated by GPC

The following general procedures apply for all experiments and lab activities.

Weighting and pipetting:

Solids were weighed on an analytical balance ([d] = 0.01 mg) with single-use spatulas onto a weighting boat. Volumes of liquids were measured by the corresponding sized pipette (Eppendorf®).

Glassware:

All glassware (incl. septum, stirring bars, caps) used for the synthesis of polymers and storage of solvents was cleaned with acetone twice. Moisture film was removed by drying the utensils for at least 12 h at 110 °C in an oven, which were only removed directly before the experiment (caps on). Water can interfere with the polymerization reaction, as it acts as secondary initiator besides mPEG-OH and leads to formation of homopolymers.

Solvent:

In all instances DCM and THF were transferred into a smaller cleaned screw capped vial to reduce risk of contamination of the main bottle and reduce the danger while handling large volumes of solvent.

glycolide and rac-lactide:

Both chemicals are highly susceptible to hydrolysis and excess of moisture entering the bottle should be avoided. glycolide and rac-lactide are removed from the fridge/ freezer 1 h prior to handling to avoid water condensing on the cold surface, when opened. Both chemicals were exposed to the ambient air for as short as possible (~20 s).

mPEG:

Prior to using mPEG (2,000 g/mol, 5,000 g/mol, 10,000 g/mol), the required amount was dissolved in anhydrous DCM (3 mL) over 5 mg magnesium sulfate in 5 mL centrifuge tubes. This allowed the removal of residual water from the mPEG.

Polymer/NPs samples:

To increase the stability of NPs solutions and prevent polymer degradation all samples were stored in a closed vial in the fridge at 4 °C whenever possible.

3.2 Radical polymerization of hydroxylated Poly(acrylic acid)

The procedure of the radical polymerization of hydroxylated poly(acrylic acid) was adapted from Xue et al. [50] and Ahmadi et al. [48]. A 100 mL 2-neck round bottom flask with a stirring bar (Ø = 30mm) was fixed to a stand above a stirring plate. Subsequently 25 mL THF, 7 mL acrylic acid (AAc), 260 µL ME and 2.5 mL Azobis(isobutyronitril) (0.2 M AIBN in toluene) were added to the flask. A condenser was added to the middle neck (cooled to 8 °C). The flask was closed with a septum and stirred at 400 rpm. The solution was bubbled with nitrogen for 30 min by adding a long needle to the bottom of the flask (short neck) and short needle on the top for pressure release (Figure 10: left). The free radical polymerization was initiated by submerging the round bottom flask into a 65 °C oil bath at low nitrogen flow, 400 rpm stirring for 22 hours. The reaction was quenched by submerging the flask in a cold-water bath.

The solution was transferred to a storage vial and some of the THF was left to evaporate in the fume hood. Before solidifying 4 mL (2-3 g PAA) of viscous solution was pipetted dropwise into 40 mL cold (-20 °C) diethyl ether in a centrifuge tube. Shaking for 3 min yielded a white precipitate. By centrifuging for 5 min with 3,500 rpm the polymer was mostly separated from the diethyl ether. After decantation the polymer was first dried in a glass petri dish at room temperature in the fume hood for 12 h followed by drying in a vacuum oven (105 °C) for 24 h, which then resulted in a white powder.

3.3 $Sn(Oct)_2$ catalyzed ring-opening polymerization of PAA-PLGA

The procedure of the ROP of hydroxylated poly(acrylic acid) with PLGA was adapted from Xue et al. [50] and Ahmadi et al. [48]. A round bottom flask (50 mL) was prepared with 1 g of PAA-OH, 1 g of LA, 0.5 g of GA and a stirring bar (Ø = 15 mm). The flask was closed with a septum and purged for 10 min with nitrogen (Figure 10: left). The flask was submerged into a 130 °C oil bath under continuous stirring (400 rpm) and purging for 20 minutes to allow the solids to melt. 50 mg $Sn(Oct)_2$ in 100 µL toluene was prepared in a small glass vial. The ROP reaction was performed for 12 h after the injection of $Sn(Oct)_2$. The polymerization was quenched by submerging the flask in a cold-water bath. The viscous product was transferred from the round bottom flask to a storage vial by dissolution in THF.

Figure 10: Nitrogen purging setup for PAA-OH/ PAA-PLGA and PEG-PCL (left); semi-batch addition of glycolide in THF to lactide, PEG and DBU dissolved in DCM.

3.4 DBU-catalyzed ring-opening polymerization of mPEG-PL(G)A

PEG-PLA:

The general procedure of the ring-opening polymerization of PEG-PLA was performed following the protocol of Qian et al. [5]. An oven-dried vial (50 mL) was clamped to a stand above a stirring plate. A stirring bar (Ø = 13mm) was added. After adding the corresponding amount of dry mPEG-OH and rac-lactide (Table 3) into 22 mL DCM, the vial was closed with a septum. Monomer and macroinitiator were dissolved by stirring (1,000 rpm) for 5 min. 37.2 µL DBU (2.5 x mol % compared to -OH) were added to 2 mL of DCM in a small glass vial. It was drawn up into a 3 mL polypropylene syringe and injected through the septum into the reaction vessel. Instantly the reaction was performed at a stirring rate of 1,500 rpm and was terminated after 90 min with 150 mg benzoic acid. After termination the solution was stirred for 5 min at 1,000 rpm.

The polymer solution was left to partially dry in the fume hood for ~48 h (NMR sample taken for conversion determination). The polymer was redissolved in 1 mL of DCM and precipitated by dropwise addition to 40 mL cold 2-propanol in a centrifuge tube. After shaking for 3 min the precipitate was filtered through a Büchner funnel (Whatman Grade 42) for 5,000g/mol and 10,000 g/mol PEG or separated by centrifuging and decantation for 2,000 g/mol PEG. The polymer was left to dry at RT in a fume hood for 24 h followed by drying in a vacuum oven at 50 °C for 24 h. The resulting white polymer powder was weighted, and the yield calculated.

PEG-PLGA:

The general procedure of the ring-opening polymerization of PEG-PLGA was performed following the protocol of Qian et al. [5] and Alanko [34]. The procedure was like the previously described PEG-PLA synthesis. An oven-dried glass vial (50 mL) with a small stirring bar (Ø = 13 mm) was clamped to a stand above a stirring plate and sealed with a septum, whenever possible. Three solutions were prepared directly prior to the synthesis (Figure 11 and Figure 10: right).

Solution 1:

Prepared inside the 50 mL glass vial. 22 mL DCM was added with a pipette to the reaction vessel. Then the calculated amount of rac-lactide and mPEG-OH was added from a weighing boat (Table 1). The solution was stirred for 5 min at 1,000 rpm to dissolve monomer and macroinitiator.

Solution 2:

Prepared inside a 6 mL capped glass vial. 37.2 µL DBU (2.5 x mol % compared to -OH) DBU was added to 2 mL DCM (mechanical pipette) and taken into a 3 mL polypropylene syringe.

Solution 3:

Prepared inside a screw-capped vial. The calculated amount of glycolide was dissolved in 6 mL of THF by 5 min of stirring with a stirring bar (Ø = 13 mm). The solution was taken into a 20 mL syringe. The syringe was added to the syringe pump (syringe calibration performed: FNP protocol) and the bended needle was introduced through the septum into the reaction vial.

The solution in the reaction vial was stirred rapidly (1,500 rpm) followed by the injection of solution 2 through the septum with a needle. Immediately after the syringe pump with the THF-glycolide was started at a rate of 0.6 mL*min^{-1}. glycolide was added dropwise over the course of 10 min. After a total reaction time of 90 min the stirring was reduced to 1,000 rpm, the septum was opened, and 150 mg benzoic acid was added to arrest the reaction. The solution was stirred for 5 min. The polymer was precipitated in 2-propanol similar to the procedure described for PEG-PLA.

Kinetic experiment for the synthesis of PEG-PL(G)A:

To understand the conversion of PLA and PLGA over the reaction time, the kinetic of the ROP was observed by taking ~300 µL of solution with a syringe in time intervals of few minutes (Table 3). The aliquots were directly transferred to a small 1 mL glass vial with 3-5 mg of benzoic acid in 300 µL DCM to terminate the reaction. The samples were analyzed in proton NMR (H1) and the ratio of free rac-lactide monomer to PLA polymer was determined against the reaction time (Figure 11).

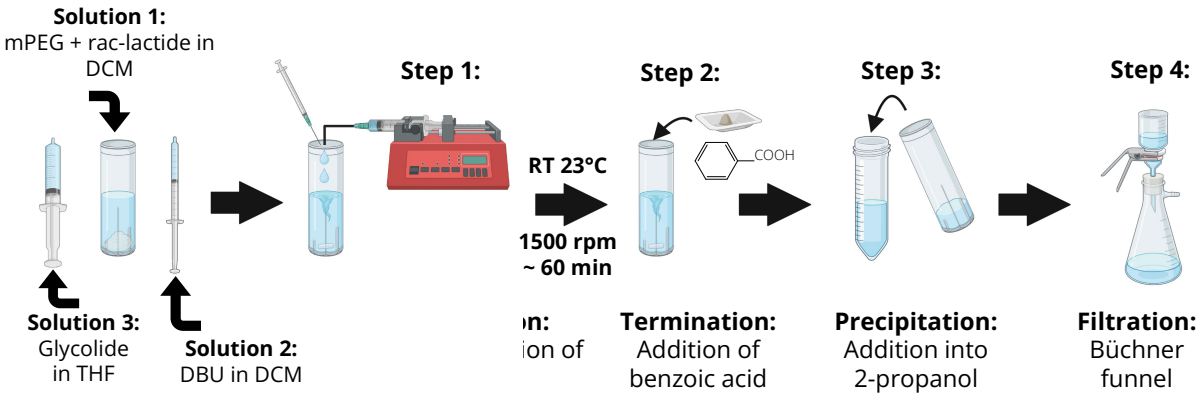

Figure 11: Synthesis of PEG-PLGA by a semi-batch process.

Table 3: Monomer ratios used for synthesis of PEG-PLGA polymers.

Polymer	PEG (mg)	rac-LA (mg)	GA (mg)	DBU (µL)	DCM (THF) (mL)
Kin. 1 PEG_{5K}-$PLA_{7.5K}$	400	600	-	29,8	24 (-)
Kin. 2 PEG_{5K}-$PL_{7.5K}G_{2.5K}A$	400	600	200	29,8	24 (6)
PEG_{2K}-PLA_{10K}	200	1000	-	37,2	26 (-)
PEG_{5K}-PLA_{10K}	500	1000	-	37,2	26 (-)
PEG_{10K}-PLA_{10K}	1000	1000	-	37,2	26 (-)
PEG_{2K}-$PL_{7.5K}G_{2.5K}A$	200	750	250	37,2	26 (6)
PEG_{5K}-$PL_{7.5K}G_{2.5K}A$	500	750	250	37,2	26 (6)
PEG_{10K}-$PL_{7.5K}G_{2.5K}A$	1000	750	250	37,2	26 (6)

3.5 DBU-catalyzed ring-opening polymerization of mPEG-PCL

The DBU-catalyzed ROP of PCL was performed following the methods presented in literature [41, 66]. A round bottom flask (50 mL) was prepared with 1.5 g of dried PEG_{2K}, 1.5 g of CL and a stirring bar (Ø = 15 mm). 114 µL of DBU (1 x mol % compared to -OH) was added to the reaction vessel. The round bottom flask was closed with a septum and bubbled with nitrogen for 10 min by adding a long needle to the bottom of the flask and short needle on the top for pressure release (Figure 10: left). While bubbling the flask was submerged into an oil bath heated to 85 °C. The stirring was set to 400 rpm and the reaction continued for 24 h. One hour into the reaction the needles were removed, and bubbling stopped. The reaction was terminated by the addition of 100 mg of benzoic acid and stirred until dissolved. The polymer was removed from the flask by dissolving in 3 mL of DCM and precipitated by dropwise addition to 40 mL cold diethyl ether into a centrifuge tube.

3.6 Polymer particle formation by FNP

For the particle formation with FNP, the established procedure from previous research was used [64]. As a reactor for FNP, the MIVM with two inlets was used (Figure 12: left). The FNP setup consisted of two syringe pumps, one for the aqueous anti-solvent and one for the organic solvent. Pre-calibrated pumps were placed above the reactor to enable a continuous flow (Figure 12: right).

Solution 1 (antisolvent):

A 1000 mL solution was prepared in a beaker by dissolving 0.1 v/v% Tween80© in MQ water. The solution was stirred at 400 rpm for 10 min until Tween80© was completely dissolved. 120 mL was drawn up into a corresponding syringe and placed in the FNP set-up.

Solution 2 (solvent):

1 wt% of polymer and 5 mg of oleic acid-coated IONPs in THF (Ø=13mm; thermal decomposition provided by PEC Group) was dissolved in a total of 12 mL of THF by vortexing for 2 min followed by 5 min of sonification. Shortly before the reaction, the solution was drawn up into a 20 mL syringe and placed in the FNP set-up.

For the start of the experiment, both pumps were started at the same time with a flow ratio of 10 : 1 (anti-solvent : solvent), while the anti-solvent pump was set to the maximum flow rate of 100 mL*min^{-1}. After establishing a flow equilibrium throughout the first 30 s of the reaction, three samples of 5mL nanoparticle containing product were transferred into small vials at an interval of 5 s. Afterwards the pumps were stopped, and the reactor was cleaned by flushing with 10 mL THF. After each experimental batch the reactor was opened, and the inside was thoroughly cleaned. Different tubes were used for experiments with IONPs and bare polymeric NPs to avoid any cross contamination.

Figure 12: Inside view of MIVM (right) for FNP; FNP setup (left) with both syringe pumps for aqueous and organic phase.

3.7 Methods for the characterization:

For characterization of the polymer samples TGA, NMR, GPC and FTIR were performed. The analysis of the polymeric NPs produced by FNP was done through DLS and STEM. Procedures and Parameters used are listed below.

FTIR:

Thermo Scientific Nicolet iS50 FT-IR with a golden gate diamond attenuated total reflectance (ATR) module was used. 5 mg of sample powder was placed on the ATR crystal und screwed down with a cone geometry until a good signal was received. A method with 2 cm^{-1} resolution and 100 scans was used. Afterwards the sample was removed, and the crystal was cleaning afterwards with ethanol.

TGA:

The TGA for all polymer samples was performed by weighing 5 mg of dried sample into the flame cleaned ceramic crucible. For Analysis in Netzsch TG209F1 the sample was heated at a rate of 20 °C/min from room temperature to 500 °C and afterwards cooled with 40 °C/min back to room temperature. The crucible was cleaned by holding into the flame of a heat gun for 1 min.

GPC:

6 mg of polymer sample was dissolved in 2 mL THF. The sample was syringe-filtered and transferred into a 1 mL HPLC vial. Agilent 1260 Infinity II was used with the refractive index detector. The molecular weight was determined automatically by the Agilent GPC/SEC software with a polystyrene calibration curve.

NMR:

NMR samples were prepared by dissolving ~40 mg of sample in 650 µL deuterated dimethylsulfoxide (*d6*-DMSO) in a small glass vial (5 mL). Dissolution rate was increased by heating to ~40 °C followed by 1 min vortexing and 1 min sonification. 600 µL were pipetted in a standard NMR tube and capped. The samples were analyzed in a Bruker Neo 600MHz instrument with two different methods at 25 °C. Proton H1 NMR and Carbon C13 NMR (512 scans, without decoupling) were used. The NMR tubes were cleaned twice with acetone afterwards and reused only for similar polymer samples. Acetone is used as it does not overlap with any sample peak. A list of all identified NMR peaks is given in the appendix (Table 7).

DLS:

The nanoparticles produced by FNP were directly analyzed in the DLS (Anton Paar Litesizer 500) apparatus. 800 µL of FNP NPs suspension were filled into a capped polystyrene disposable cuvette and the hydrodynamic size measurement was started (25 °C, max. 60 runs @ 10 s, automatic). Zeta potential for the NP solution was measured in an OMEGA®

cuvette. Afterwards the cuvettes were flushed three times with 10 mL MQ water to remove the previous sample.

S(T)EM:

Grids were prepared by taking a formvar-coated copper grids (carbon site upwards) with a cleaned forceps and placing it on the bench. 10 µL of the NP suspension were placed on the carbon grid with a mechanical pipette. The grid was left to dry for 30 min and residual sample was removed by a wet tissue paper. Next, 6 µL of 1 % phosphotungstic acid (PTA) stain (pH ~7.0) was placed on the grid and left for ~1 min before being removed by a wet tissue. Grids were then analyzed with a NTNU NanoLabs Hitachi S-5500 instrument at different magnifications. Energy-dispersive X-ray spectroscopy (EDX) was performed to confirm PTA and IONPs in the STEM images.

Software:

All graphs and calculations of derivatives, mean values and standard derivations were done by the software Origin 2023 from OriginLab®. NMR data was analyzed and visualized by the software MestreNova®. For image processing and particle measurements, the ImageJ2 distribution Fiji® was used. General schemes and graphical pictures were prepared with the help of BioRender®, CorelDraw®, ChemDraw® and Adobe Photoshop®.

4. Results and discussion

4.1 Synthesis of PEG-PLA block-copolymer

For the preparation of the PEG-PLA block-copolymer, the method used by Quin et al. was employed [59]. The ratios of the hydrophilic mPEG block and hydrophobic PLA block were varied using different commercial molecular weight mPEG (M_n = 2K, 5K and 10K g/mol) as macroinitiators. For the DBU-catalyzed ROP of rac-lactide as monomer, a M_n of 10,000 g/mol was targeted. The three weight ratios PEG_{2K}-PLA_{10K} (1 : 5), PEG_{5K}-PLA_{10K} (1 : 2) and PEG_{10K}-PLA_{10K} (1 : 1) were polymerized. During the polymer precipitation the dropwise addition of the lowest molecular weight PEG_{2K} in cold 2-propanol did not result in a fine suspension. As the monomer rac-lactide and low M_w PLA are both soluble in 2-propanol, the low ratio of PEG to PLA in the block-copolymer could result in partial solubility. The product appeared as a sticky mass so that it could not be filtered, and the 2-propanol was decanted. After vacuum drying larger lumps were present in the PEG_{2K}-PLA_{10K} polymer sample. The yield of the polymerization for all ratios was 60-70 %, with parts of the sample lost in the filter paper. Pure water-initiated PLA impurities were washed away with 2-propanol (Table 4). PEG_{2K}-PLA_{10K} polymer sample shows the highest yield as the lack of filtration and formation of a powder left solvent residue entrapped in the lumps. A conversion of > 98 % was calculated by H1 NMR prior to filtration (Table 4). All three samples were soluble in THF. Their chemical structures and thermal properties were characterized by FTIR, NMR, GPC and TGA.

The three polymer samples PEG_{2K}-PLA_{10K}, PEG_{5K}-PLA_{10K} and PEG_{10K}-PLA_{10K} are compared to pure PEG_{5K} (Figure 13) using ***FTIR*** to confirm changes in chemical composition. At 2885 cm^{-1}, the C-H stretching of the methylene group of PEG was clearly present. With a decreasing content of PEG, the C-H peak became smaller and overlaps with the C-H stretching of the methyl group of the PLA (~2920 cm^{-1}). At 1750 cm^{-1}, the sharp C=O stretching peak of the ester group present, which resulteded from the polymerization with lactic acid, became

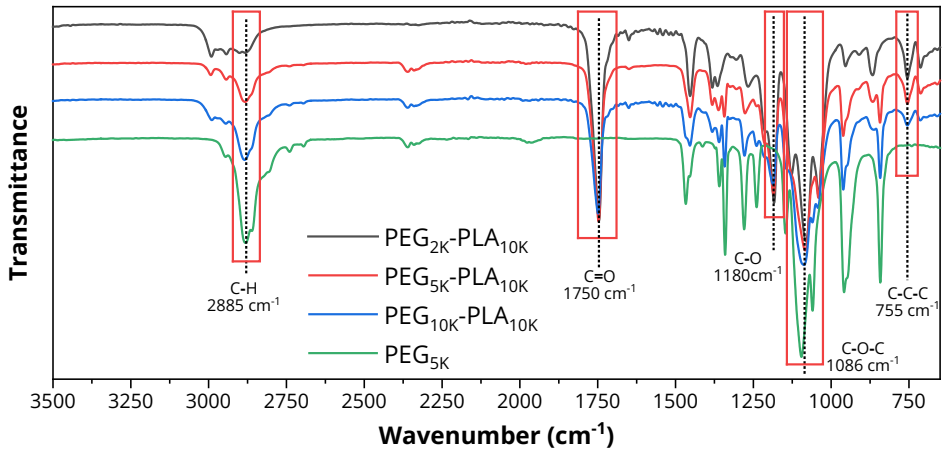

Figure 13: FTIR spectra of synthesized PEG-PLA with different molecular weight ratios between PLA and PEG.

detectable. The peak appearing around 1180 cm^{-1} corresponded to the C-O ester stretching by the polymerized lactic acid. When the PLA content increased the C-O ester stretching also increased. Around 1086 cm^{-1}, the C-O PEG ether stretching became visible for all samples. The sharp peak of the disubstituted carbon around 755 cm^{-1}, which is characteristic for lactic acid, confirmed the increase in the PLA content for the three block-copolymers. The characteristic FTIR peaks described above were also reported in previous publications [68]. In a study by David K. Wang et al., who had synthesized triblock PLA-PEG-PLA copolymers at different ratios with DBU, characteristic PEG and PLA chemical groups were detected with ATR-FTIR [69].

The thermal stability of the PEG-PLA copolymers was analyzed by ***TGA***. The weight loss was observed over the temperature range from 0-500 °C for each of the three samples (Figure 14: left). The polymers were stable up to a temperature of 200 °C. Between 200 °C and 350 °C the PLA block of the polymer degraded. After a small plateau around 375 °C, a second degradation step between 400 °C and 450 °C was identified as PEG. These assignments were supported by running reference samples of pure commercially available PEG and PLGA standards (Figure 14: right). Through calculation of the minimum rate of weight loss between the two degradation steps, the approximate weight ratio between the two blocks was determined. PEG_{2K}-PLA_{10K} (1 : 5) showed a PEG content of 19.5 %, which corresponded with the expected value. PEG_{5K}-PLA_{10K} (1 : 2) and PEG_{10K}-PLA_{10K} (1 : 1) both showed a slightly increased PEG content of 38.4 % and 57.2 %, respectively. This can be explained by some polymerization of the PLA homopolymer as well as by unconverted monomers, that were washed away during the filtration step. When comparing our TGA results to data on PEG-PLA reported in the literature, a similar two-step degradation behavior at ~300 °C for PLA and ~400 °C for PEG was observed for different weight ratios of stannous octoate-catalyzed PEG-PLA [70].

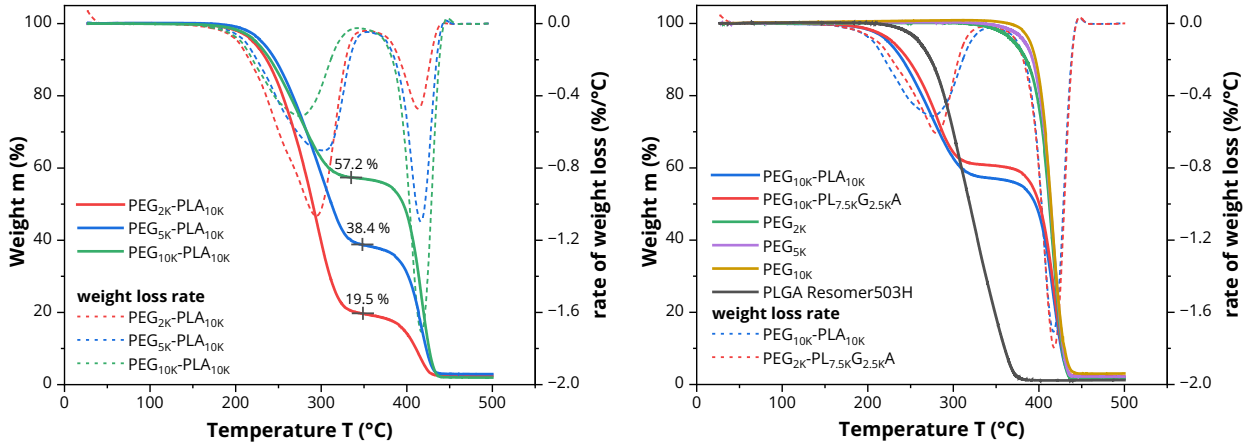

Figure 14: TGA analysis of PEG-PLA for different PEG:PLA ratios, calculated PEG weight content marked with cross (left); comparison of PEG-PLA. PEG-PLGA, pure PEG and pure PLGA (right).

Proton H1 NMR was used to identify the chemical structure of the three PEG-PLA block-copolymers in d6-DMSO (2.5 ppm). The different peaks were assigned to the corresponding protons in the chemical structure of PEG_{5K}-PLA_{10K} after washing (Figure 15). The broad methanetriyl peak (CH) of PLA was visible at 5.20 ppm, while the LA monomer methanetriyl peak (A1: CH) at 5.45 ppm was absent from the spectra (Appendix: 6.2 NMR monomer reference spectra). DBU-LA complexes were not visible in the range of 3.75 ppm – 5.0 ppm. The washing process with 2-propanol successfully removed the monomer and the catalyst. At 1.46 ppm, the three-proton methyl group (A2: CH3) of PLA was confirmed by having thrice the integral value compared to the single proton A1. The methylene group (C: CH2) of PEG was clearly visible at 3.51 ppm and confirmed by running a reference spectrum of bare PEG (Appendix: 6.2 NMR monomer reference spectra). Successful block-copolymerization was verified by the shift to 4.20 ppm (B: CH2) due to the PEG methylene group neighboring the PLA end group. The linkage (B: CH2) was reported for PEG-PLA diblock and triblock copolymers synthesized with DBU [59] or stannous octoate [71]. The methanetriyl end group of PLA at 4.20 ppm (E: CH) was overlapping with peak B. Integration of the two groups (B+E) gives 6.90 protons per PEG-PLA molecule, when the theoretical end group of mPEG was assumed. The theoretical expected value was 3 protons per molecule. Differences between the two values could indicate synthesis of pure PLA besides the block-copolymer. At 3.24 ppm the methyl end group of the PEG (D: CH3) was identified. The peak was overlapping with the broad water resonance at 3.32 ppm, which was introduced with the washing of the polymer in technical grade water containing 2-propanol. An additional unknown triplet peak was overlapping with D. The adjacent peaks alter the integral of D compared to the pure PEG H1 NMR spectra (Appendix:6.3 NMR spectra of PEG-PL(G)A samples). For the molecular weight analysis, the PEG (C: CH2) peak was chosen over the methyl end group D.

The molecular weight of the different block ratios was determined with ***H1 NMR and GPC*** (Table 4). From the initial monomer concentration, the theoretical number average molecular weight $M_{n\ theo}$ with the assumption of a maximum conversion and a $Đ_m$ of 1 was calculated. For the calculation of the H1 NMR number average molecular weight ($M_{n\ H1\ NMR}$) by end group analysis the methylene group (C: CH2) of the commercial PEG was used. The total proton count/$M_{n\ H1\ NMR}$ of PEG was calculated from the methyl end group (D: CH3) of the bare PEG reference sample mentioned above. The integral of PLA A1 represents the degree of polymerization (DP) of the monomer LA. Multiplying the DP with the molecular weight of the monomer and adding the PEG molecular weight results in $M_{n\ H1\ NMR}$ (Appendix: 6.3 NMR spectra of PEG-PL(G)A samples). $M_{n\ H1\ NMR}$ is lower than $M_{n\ theo}$ for all block-copolymer ratios. The difference for PEG_{2K}-PLA_{10K} and PEG_{5K}-PLA_{10K} can be explained by a conversion of < 100 % and by some impurities, like water-initiated low M_n homopolymer PLA. A comparison between the PEG normalized H1 NMR before and after washing accounts for 5 % to 10 % of PLA being removed with 2-propanol lowering the maximum $M_{n\ NMR}$ (Appendix: 6.3 NMR spectra of PEG-PL(G)A samples). In case of PEG_{10K}-PLA_{10K}, a difference of 4,000 g/mol was

calculated between $M_{n\ Theo}$ and $M_{n\ NMR}$. The larger molecular weight of the PEG_{10K} led to lower reaction rates compared to the more mobile, low M_n and impurity-initiated PLA chains. The number of monomers taking part in the actual PEG_{10K}-PLA_{10K} synthesis is smaller than for lower PEG_{2K} and PEG_{5K} block-copolymerization.

The weight average molecular weight ($M_{w\ GPC}$) and polydispersity ($Đ_m$) of the different ratios were analyzed by ***GPC***. The $M_{w\ GPC}$ was for all cases lower than the theoretical value calculated. The $Đ_m$ showed a narrow distribution of 1.1 for PEG_{5K}-PLA_{10K} and PEG_{10K}-PLA_{10K}. PEG_{2K}-PLA_{10K} had a broader range with $Đ_m$ of 1.4. The low values indicated the presence of a living polymerization. Mechanism like nucleophilic transesterification and acylation were absent in these reaction conditions [40, 53]. The expected values for the DBU-catalyzed polymerization reported in the literature was around 1.1 in the presence of an excess amount of hydroxyl groups ([-OH] : [DBU] > 1.5 - 2.0) [40, 59]. As for PEG_{2K}-PLA_{10K} presence of impurities promoting some secondary initiation or nucleophilic transesterification could cause the higher $Đ_m$.

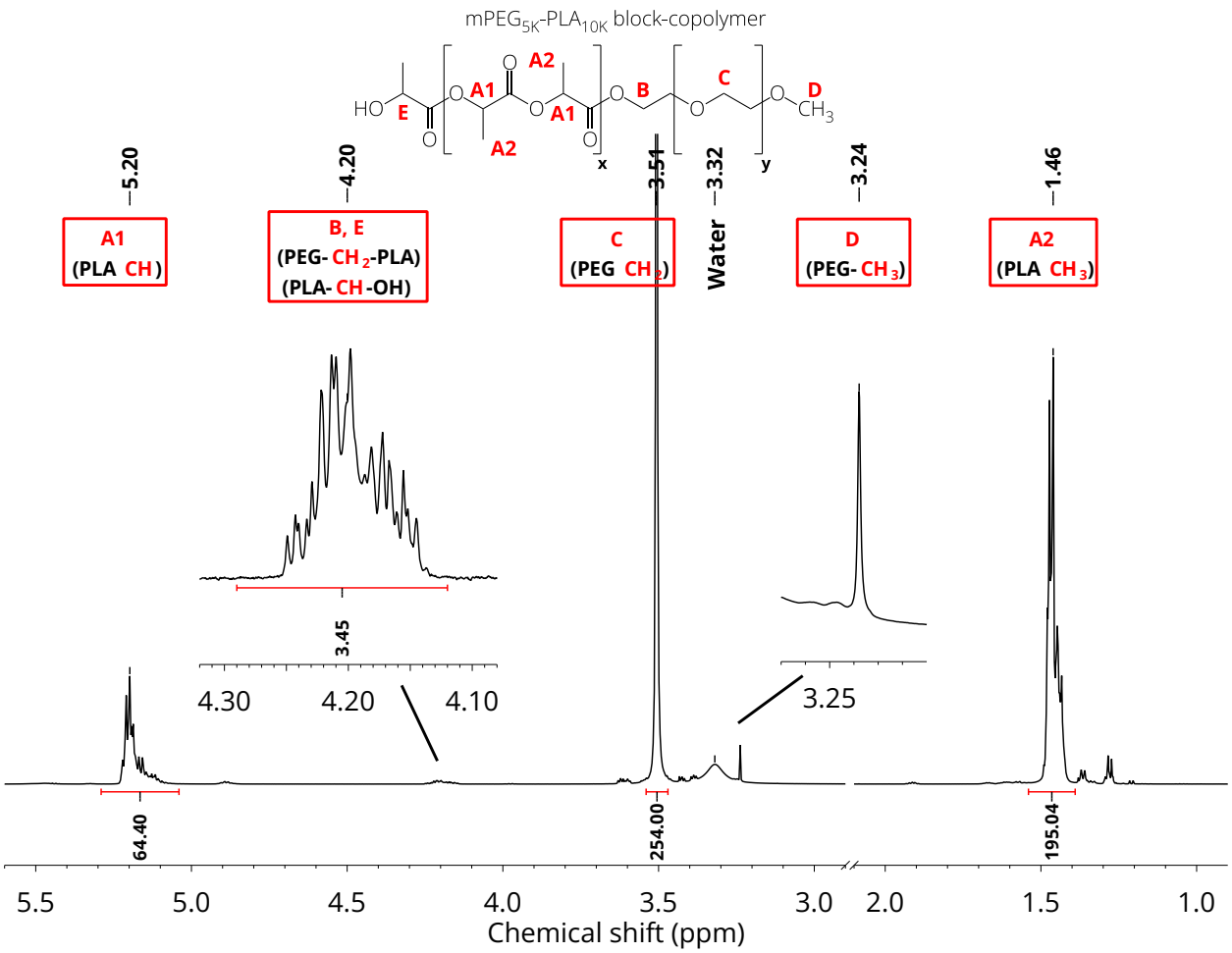

Figure 15: Proton H1 NMR of PEG_{5K}-PLA_{10K} in *d6*-DMSO (2.50ppm); Peak B (PEG-PLA) (4.20ppm) methanediyl link between PEG-PLA; Integrals are normalized towards the DP of LA.

Table 4: Comparison of yield, conversion (conv.) and molecular weight of PEG-PL(G)A block-copolymers prepared by DBU-catalyzed ROP.

Polymer	Yield* (%)	Conv. LA** (%)	$M_{n\ Theo}$ (g/mol)	$M_{n\ H1\ NMR}$*** (g/mol)	$M_{w\ GPC}$ ($Đ_m$) (g/mol)
Kin. 1 PEG_{5K}-$PLA_{7.5K}$	-	89	12,500	11,248	11,700 (1.1)
Kin. 2 PEG_{5K}-$PL_{7.5K}G_{2.5K}A$	-	90	15,000	13,664	12,000 (1.1)
PEG_{2K}-PLA_{10K}	80	99	12,000	11,027	6,500 (1.4)
PEG_{5K}-PLA_{10K}	64	99	15,000	14,916	13,400 (1.1)
PEG_{10K}-PLA_{10K}	61	97	20,000	16,109	17,000 (1.1)
PEG_{2K}-$PL_{7.5K}G_{2.5K}A$	81	96	12,000	9,531	N/A
PEG_{5K}-$PL_{7.5K}G_{2.5K}A$	93	98	15,000	14,382	12,000 (1.1)
PEG_{10K}-$PL_{7.5K}G_{2.5K}A$	53	76	20,000	15,491	16,300 (1.1)

*Calculated by mass balance after washing with 2-propanol and drying.
**Calculated by H1 integral ratio of P(LA) methine peak (PLA: 5.20 ppm; LA: 5.45 ppm) in *d6*-DMSO.
***Determined by end-group analysis (PEG 3.57 ppm + methyl group 3.30 ppm) in *d6*-DMSO.
(NMR spectra and calculations: Appendix 6.4 NMR Graphs of PEG-PL(G)A samples)

4.2 Synthesis of PEG-PLGA block-copolymer

The polymerization of PEG-PLGA followed a similar procedure as described by Qian et. al. for PEG-PLA [59]. $mPEG_{2K}$, $mPEG_{5K}$ and $mPEG_{10K}$ were copolymerized with glycolide and rac-lactide in a semi-batch process catalyzed by DBU. Preliminary experiments suggested that polymerization of a completely random 50:50 wt% rac-lactide to glycolide ratio resulted in early precipitation during synthesis. The resulting polymer was insoluble in THF due to large continuous glycolide blocks [64]. Therefore, the targeted PLGA copolymer ratio was reduced to 75:25 wt% LA to GA. Glycolide dissolved in THF was added in a constant rate over the first 10 min of the reaction. Block-copolymers PEG_{2K}-$PL_{7.5K}G_{2.5K}A$, PEG_{5K}-$PL_{7.5K}G_{2.5K}A$ and PEG_{10K}-$PL_{7.5K}G_{2.5K}A$ were successfully polymerized by the semi-batch method. The resulting PLGA is assumed to form a semi-random gradient copolymer with the glycolide content decreasing throughout the reaction. The higher molecular weight PEG_{10K}-$PL_{7.5K}G_{2.5K}A$ precipitated in the DCM/THF reaction solution after 20 min. The reaction resulted in a low conversion of 76 % LA and a yield of only 53 % (Table 4). The resulting polymer was only partially soluble in THF demonstrating the limitation to a molecular weight < 20,000 g/mol for the DBU-catalyzed ROP. Like PEG-PLA the low molecular weight PEG_{2K}-$PL_{7.5K}G_{2.5K}A$ did not precipitate as a homogenous suspension during the washing step. Decantation instead of filtration was used. For PEG_{2K}-$PL_{7.5K}G_{2.5K}A$, PEG_{5K}-$PL_{7.5K}G_{2.5K}A$ the lower solubility of the product in 2-propanol resulted in a higher yield compared to PEG-PLA. The conversion was above 95 % (Table 4). Both polymers were soluble in THF.

The chemical structure and properties of the PEG-PLGA block copolymers were characterized by means of FTIR, H1 NMR, GPC and TGA (Figure 16: C). ***FTIR*** analysis confirmed the additional glycolide methylene group (CH_2) by the broadening of the alkane C-H stretching at 2885 cm^{-1}. The corresponding methylene bending from GA appeared around 1400 cm^{-1}. These characteristic glycolide absorbance peaks were previously also seen with PGA and PEG-PLGA produced from $Sn(Oct)_2$ [72, 73]. Peaks corresponding to PEG and LA are identified and correlate to the three block copolymers PEG-PLA spectra reported for the PEG-PLA synthesis.

TGA graphs were obtained for the three ratios showing a two-step thermal degradation pattern (Figure 16: B). The random copolymer PLGA degraded between 200 °C to 300 °C, while PEG decomposed between 400 °C to 450 °C. When comparing PEG_{10K}-PLA_{10K} with PEG_{10K}-$PL_{7.5K}G_{2.5K}A$ and commercial 50:50 PLGA (Figure 14: right) an increase in degradation temperature was observed. With higher glycolide content, the polymer was more densely packed and the crystalline domains increased. More thermal energy was required to break down the polymer. An analogous behavior has been reported by others for different ratios of LA and GA in PLGA random copolymer produced by $Sn(Oct)_2$ [74]. Both PEG_{2K}-$PL_{7.5K}G_{2.5K}A$ and PEG_{5K}-$PL_{7.5K}G_{2.5K}A$ polymer lumps contain 3.5 wt% and 2.2 wt% residual solvent, respectively, as a left over from the washing step. Drying in the vacuum oven at 50 °C for 24h

was not sufficient to remove solvents trapped in the polymer clumps. The weight ratio between PEG and PLGA was calculated from the minimum rate of weight loss between the steps. The solvent residues were considered for PEG_{2K}-$PL_{7.5K}G_{2.5K}A$ and PEG_{5K}-$PL_{7.5K}G_{2.5K}A$. With increase in the PEG molecular weight, a loss of PLGA through lower conversion and polymerization of PLGA homopolymer was observed. With 22.7 wt% (1 : 5), 39.9 wt% (1 : 2) and 57.2 wt% (1 : 1) the content of PEG in the samples was similar to PEG-PLA. The addition of glycolide did not have an impact on the weight ratio obtained by TGA.

H1 NMR was used to identify the chemical groups of the PEG_{5K}-$PL_{7.5K}G_{2.5K}A$ block-copolymer (Figure 15: A) (6.3 NMR spectra of PEG-PL(G)A samples). With the addition of glycolide, the methylene resonance (B: CH2) around 4.91 ppm corresponding to PGA appeared. The methylene resonance of the glycolide monomer at 5.05ppm (Appendix: 6.2 NMR monomer reference spectra) was not detectable, indicating a 100% conversion to the polymer. LA and PLA peaks remain unaltered compared to PEG-PLA discussed above. The proton resonance of the PEG methylene group (C: 4.21 ppm // 4.12 ppm) linking the PEG to PLGA showed a peak broadening compared to PEG-PLA. PEG connected to a PGA unit had lower nuclear

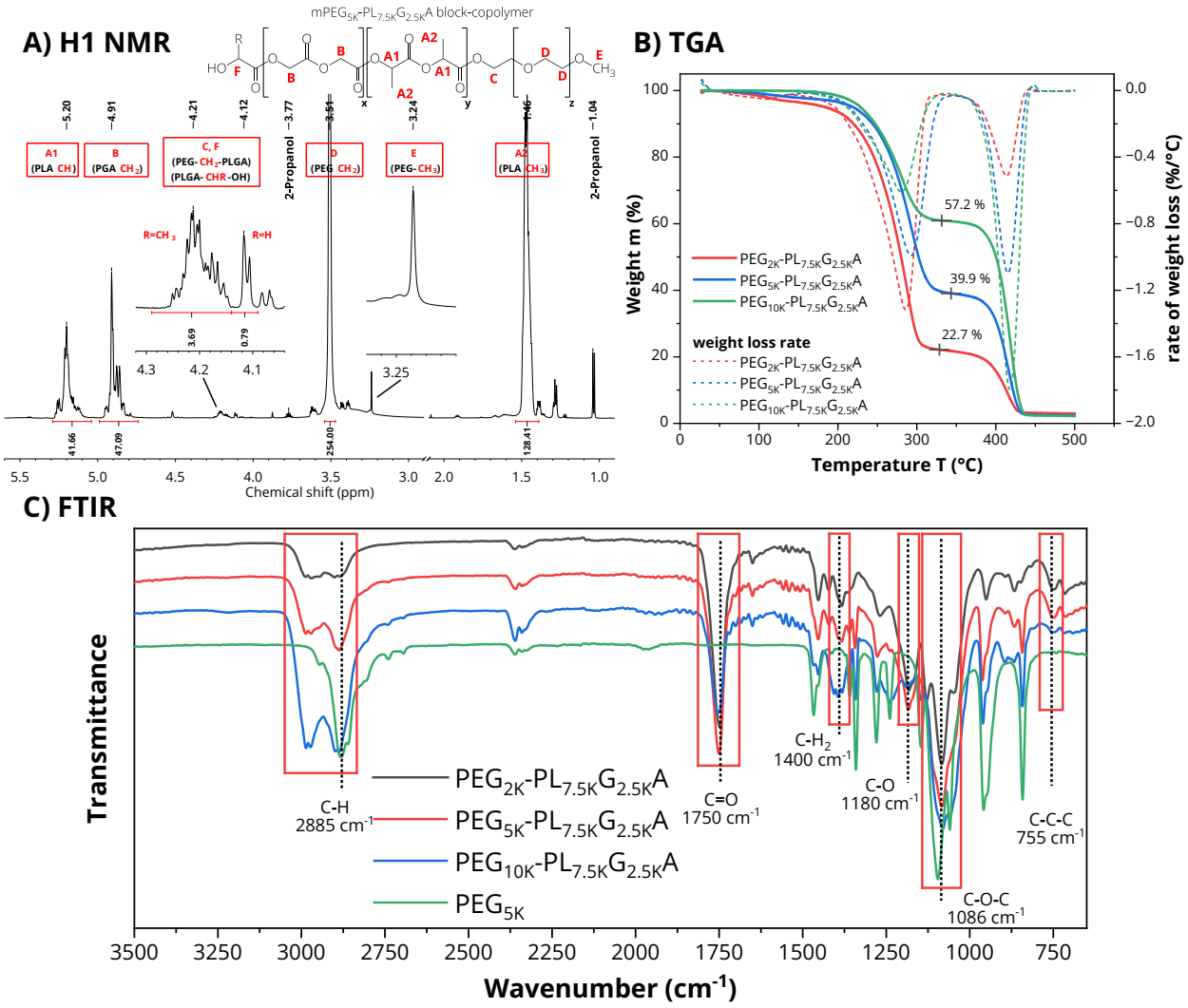

Figure 16: Different PEG-PLGA ratio analysis by A) H1 NMR, B) TGA and C) FTIR.

resonance (C: 4.12 ppm R=H) compared to PEG connected to PLA (C: 4.21 ppm R=CH3). Both groups GA and LA were involved in the initiation of the polymerization from the mPEG.

In the feed of the reaction a ***molar ratio*** of 29.3 : 70.7 GA to LA was used. Using H1 NMR, the GA to LA molar ratio was calculated from the cleaned block copolymer samples (Table 4). For PEG_{2K}-$PL_{7.5K}G_{2.5K}A$ and PEG_{5K}-$PL_{7.5K}G_{2.5K}A$ the GA content in the polymer increased by ~7% compared to the molar feed composition. Around 10% percent of unreacted LA monomer or low M_n PLGA was removed in the washing step with 2-propanol. Similar loss of LA content was confirmed by the direct comparison of the H1 NMR before and after the washing. As for PEG_{10K}-$PL_{7.5K}G_{2.5K}A$ the calculated ratio between GA and LA was nearly 50 : 50, which is in accordance with the observed early precipitation during synthesis and low conversion of LA.

The ***H1 NMR and GPC*** was used to calculate the molecular weight of $M_{n\,H1\,NMR}$ and $M_{w\,GPC}$. For both values, the molecular weight was lower than the theoretical value. The $M_{n\,H1\,NMR}$ and $M_{w\,GPC}$ avalues and $Đ_m$ results align with the previously obtained PEG-PLA synthesis. Neither the addition of glycolide nor $Đ_m$ had an effect on the molecular weight. For $M_{w\,GPC}$ PEG_{2K}-$PL_{7.5K}G_{2.5K}A$ the GPC run was not successful as residual solvents led to a broad signal (Table 4).

To understand the randomness between LA and GA blocks in the polymer backbone ***C13 NMR*** was used to identify the characteristic carbon resonances. Peaks of PEG_{10K}-$PL_{7.5K}G_{2.5K}A$ were identified through the C13 NMR in *d6*-DMSO (Figure 16). The methylene carbon at 71.28 ppm (C: CH2) corresponds to the PEG backbone. The PGA methylene carbon (B: 61.19 ppm), the PLA methine carbon (A2: 69.16 ppm) and the PLA methyl carbon (A1: 19.94 ppm) were compared to a commercial PLGA sample and cross-checked with previously published data [59, 63, 75]. Monomer peaks were not visible in the PEG_{10K}-$PL_{7.5K}G_{2.5K}A$ sample. The carbonyl groups had resonances between ~167 ppm for GA and ~170 ppm for LA backbone carbons. Depending on the adjacent repeating unit, the carbonyl carbons showed a shift in resonance. GA with adjacent LA (**G**L: 167.08 ppm) had a lower value compared to GA with an adjacent GA (**G**G: 167.18 ppm). A similar shift was observed for **L**L and **L**G at 170 ppm, but the peaks were overlapping obstructing precise integration. The use of hexafluoroisopropanol in *d*-chloroform has been reported to yield more defined peaks for the analysis of the **L**L and **L**G peak of PLGA produced by DBU and $Sn(Oct)_2$ compared to *d6*-DMSO used in this research [59, 62, 76]. From the integrals, the average sequence length of GA ($\overline{L_{GA}}$) and LA ($\overline{L_{LA}}$) were calculated by Equation (8)(9) for all three PEG-PLGA ratios (Table 4). For a completely random block copolymer with a 50 : 50 molar ratio of the dimers glycolide and rac-lactide the average sequence length expected is 4 [59]. An alternating polymer would have the sequence length of 2 for GA and LA. For PEG_{2K}-$PL_{7.5K}G_{2.5K}A$ and PEG_{5K}-$PL_{7.5K}G_{2.5K}A$ the low $\overline{L_{GA}}$ of 3.90 and 3.66 suggests a random copolymerization. The semi-batch process works well for the solution polymerization of PEG-PLGA with DBU and results are similar to those reported by Qian et all. ($\overline{L_{GA}}$ = 3.00) [59]. In case of PEG_{10K}-$PL_{7.5K}G_{2.5K}A$, the higher sequence length of 5.08 explains the low solubility and precipitation during the synthesis. Quality of the polymer in regards of the randomness is on par with the commercial Resomer503H

($\overline{L_{GA}}$ = 3.05) [63] and PLGA ($\overline{L_{GA}}$ = 2.80) catalyzed by Sn(Oct)$_2$. Previous studies found and $\overline{L_{GA}}$ of 3.7 for 41.7 wt% GA [62] and 2.60 for 30 wt% GA [76] with Sn(Oct)$_2$ as catalyst. At higher molar ratios close to 50:50 DBU catalyst tends to form longer $\overline{L_{GA}}$ compared to Sn(Oct)$_2$, resulting in precipitation and limitation of the copolymerization. To further understand the reaction pathways and copolymerization behavior the reaction kinetics of DBU are investigated for the previous polymerizations.

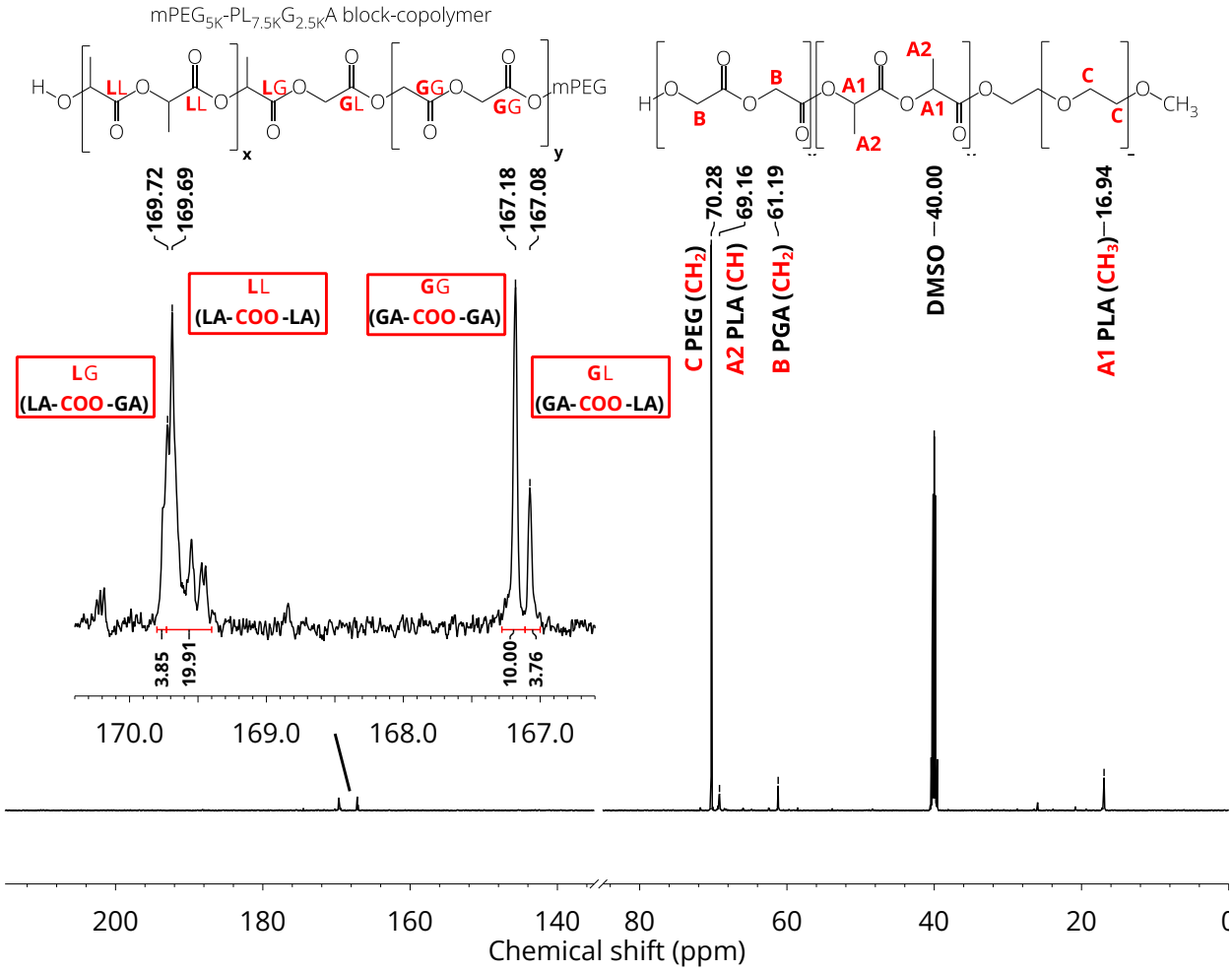

Figure 17: C13 NMR in *d6*-DMSO (40 ppm) for PEG-PLGA carbonyl carbon resonance 167 ppm – 170 ppm used for sequence length analysis; LG (169.72 ppm) peak overlap with LL (169.69 ppm).

Table 5: Analysis of PLGA average sequence block length between commercially, DBU and $Sn(Oct)_2$ produced polymer.

Polymer	Feed Molar ratio GA:LA	H1 NMR Molar ratio GA:LA*	Sequence Length $\overline{L_{GA}}$**	Sequence Length $\overline{L_{LA}}$**
PEG_{2K}-$PL_{7.5K}G_{2.5K}A$	29.3:70.7	37.3:62.7	3.90	5.42
PEG_{5K}-$PL_{7.5K}G_{2.5K}A$	29.3:70.7	36.1:63.9	3.66	6.17
PEG_{10K}-$PL_{7.5K}G_{2.5K}A$	29.3:70.7	46.7:53.3	5.08	5.40
PAA_{2K}-$PL_{2K}G_{1K}A$ ($Sn(Oct)_2$)	39.3:61.7	40.5:59.5	2.80	4.44
PLGA Resomer503H©	N/A	50.8:49.2	3.05	2.97

*Calculated by H1 integral ratio of PLA methine peak (PLA: 5.20 ppm) and PGA methylene peak (PGA: 4.91 ppm) in *d6*-DMSO.
**Calculated by C13 integral ratio of the carbonyl carbon (Equation (8)/(9)).
(NMR spectra and calculations: Appendix: 6.3 NMR spectra of PEG-PL(G)A samples)

4.3 Kinetic Study on DBU PEG-PL(G)A synthesis

A kinetic study of the copolymerization was used to identify the reaction pathways valid for the copolymerization of PEG-PL(G)A in this work. The conversion of LA to PLA was observed for similar reaction conditions as used in block copolymerization discussed before. The monomer resonance of rac-Lactide (LA: 5.43 ppm) was compared to the polymer PLA resonance (A1: 5.20 ppm) at different times throughout the reaction of PEG_{5K}-$PL_{7.5K}G_{2.5K}A$ (Figure 18). From the figure a clear decrease of LA monomer resonance and increase in PLA resonance is visible. After 60 min the total conversion reached 90 % and the reaction was arrested (Table 4). The conversion (X) was calculated for each time stamp following the equation (16). When the logarithm of the conversion was plotted against the time the reaction order can be determined. In case of a first order reaction a linear slope was expected. For both experiments Kin. 2 PEG_{5K}-$PL_{7.5K}G_{2.5K}A$ and Kin. 1 PEG_{5K}-PLA_{10K} the graph does not show a linear curve. The adjusted R^2 were below 75 %. When an exponential growth fit described the conversion over time, it gave an adjusted R^2 above 98 %. The kinetic experiment did not show a living polymerization behavior based on the AAP. The excess amount of catalyst DBU in comparison to the alcohol groups from mPEG (2.5 : 1) promoted partial NAP. The NAP reaction pathway was prone to acylation between DBU initiated chains and free hydroxyl groups. This resulted in the higher reaction rate in the start of the experiment compared to a lower rate at higher conversion. Results have been published for a ratio of 2.1 : 1 between DBU and mPEG showing similar conversion over time behavior for PEG-PLA synthesis [40]. During the semi-batch process GA was added over the first 10 min and reacts instantaneously. GA was absent in all aliquots taken from Kin. 2 PEG_{5K}-$PL_{7.5K}G_{2.5K}A$. Since a living polymerization was targeted the amount of catalyst should be reduced and the reaction time prolonged.

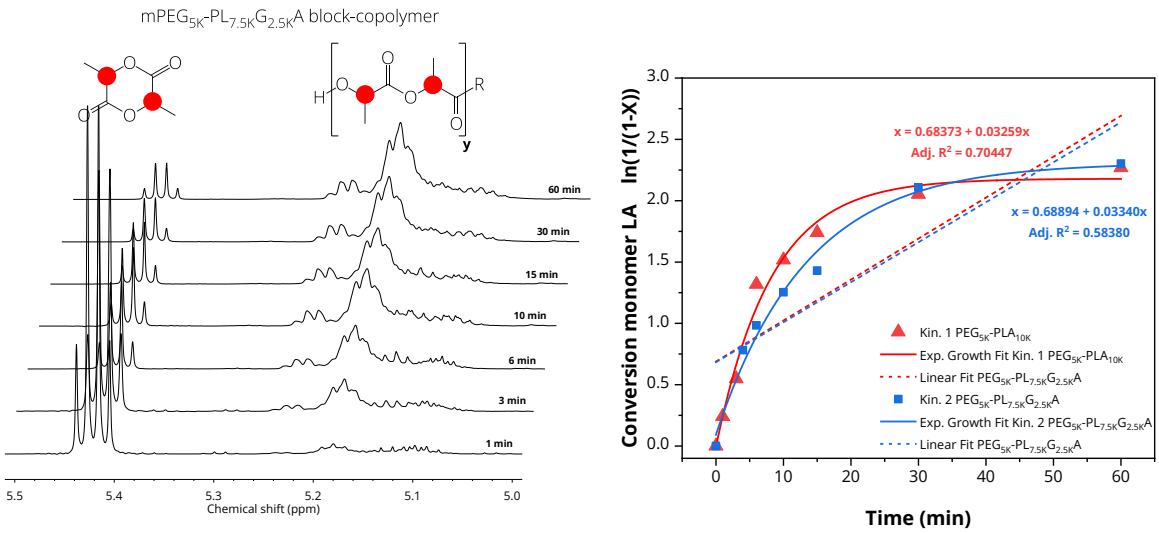

Figure 18: H1 NMR of conversion of rac-lactide monomer to PLA polymer during DBU-catalyzed synthesis of PEG_{5K}-$PL_{7.5K}G_{2.5K}A$ (left); logarithm of conversion LA (X) vs time, linear fit for first order reaction not suitable.

4.4 Synthesis of PAA-PLGA block-copolymer

The synthesis of the amphiphilic block copolymer PAA-PLGA included a two-step process, free radical polymerization of PAA-OH followed by the ROP of PLGA with stannous octoate. The free radical polymerization of hydroxyl terminated PAA-OH_{2K} was successful. After vacuum drying a white crystalline powder was obtained. The sample did not show any crosslinking of PAA-OH_{2K} and was soluble in THF and DMSO. The chemical structure and properties of the polymer were confirmed by NMR, FTIR and TGA (Figure 19).

The polymer was analyzed through ***TGA*** and showed a characteristic three step degradation behavior (Figure 19: B). The first step around 200 °C is attributed to the loss of hydrogen-bounded water from the carboxylic acid. This step also included the removal of entrapped solvent residues like THF or Toluene. For PEG-OH_{2K} around 10 wt% was residual solvent and water. The second thermal degradation step 250 °C showed the formation of anhydrides from close packed carboxylic acids. The complete degradation occurred in the range of

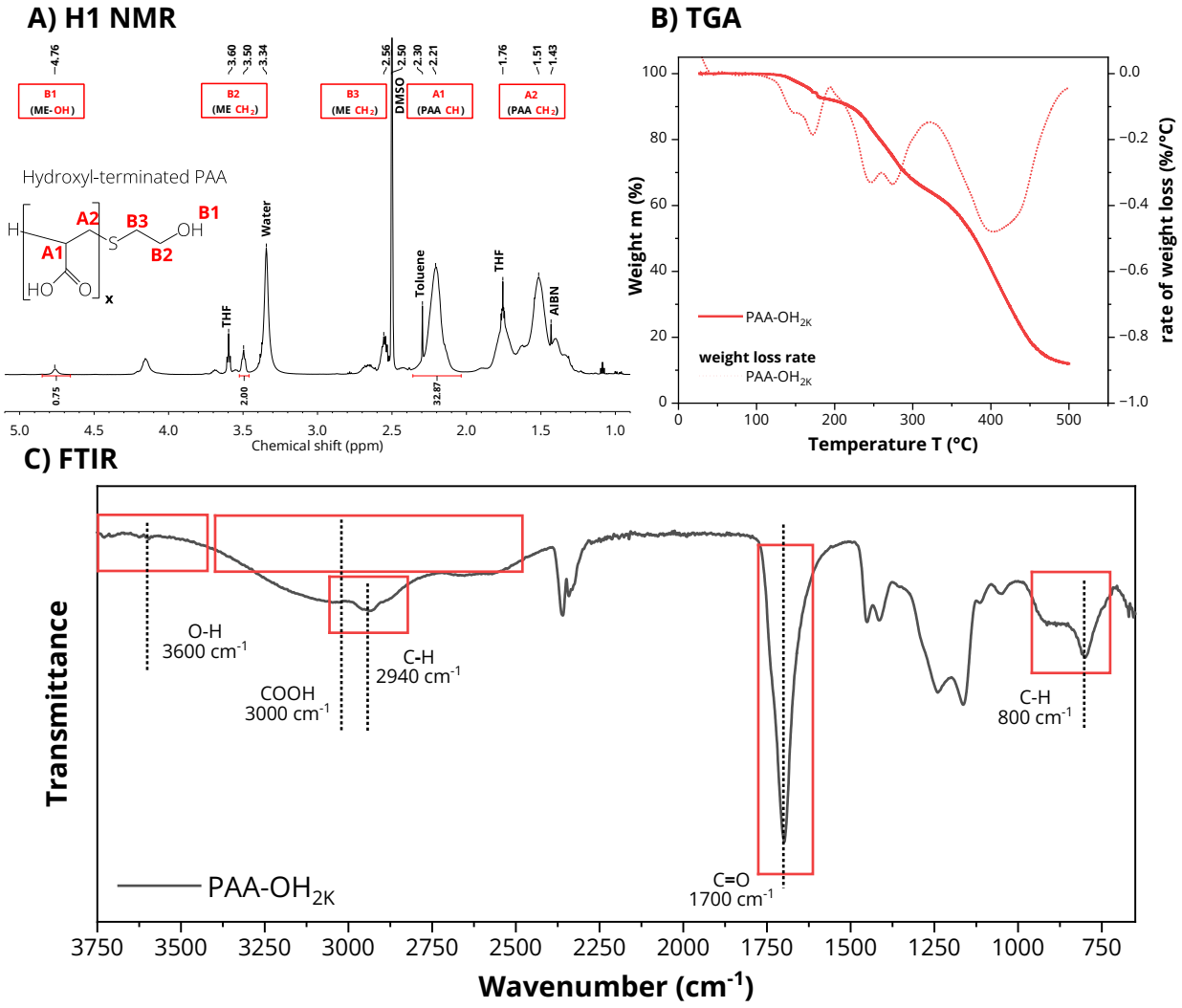

Figure 19: Characterization of polymerized hydroxyl terminated PAA-OH_{2K} by A) H1 NMR in *d6*-DMSO B) TGA and C) FTIR.

390 °C to 450 °C. This thermal degradation behavior was widely described in literature by various sources for low and high molecular weight PAA [77, 78].

The ***FTIR*** analysis of the PAA-OH powder revealed the characteristic broad absorbance peaks of the carboxylic acid around 3000 cm^{-1} (Figure 19: C). The C-H stretching at 2940 cm^{-1} as well as the C-H bending of the di- and trisubstituted carbon backbone was visible. The C=O stretching at 1700 cm^{-1} confirmed the presence of conjugated carboxylic acid groups. The peak corresponding to the hydroxyl functionalization was expected to appear around 3600 cm^{-1} showing the O-H stretching of a free hydroxyl group. A small peak visible in the spectrum was nearly out of the resolution range. Since the amount of free hydroxyl groups was very low these results were expected. The peaks corresponded to the values reported in literature for a similar PAA-OH synthesis procedure [48, 79].

H1 NMR was used to identify the chemical composition of the PAA-OH_{2K} (Figure 19: C). Two broad resonances associated with PAA were identified. The methanetriyl group (A1: 2.21 ppm) and the methylene group (A2: 1.51 ppm) were characteristic for PAA. Acrylic acid monomer peaks were absent from the spectra suggesting a high conversion to PAA (6.2 NMR monomer reference). PAA was successfully functionalized with ME and the free hydroxyl group resonance showed at 4.76 ppm (B1). The two methylene groups of ME (B2: 3.50 ppm/B3: 2.56 ppm) showed a small shift compared to the reference spectra. The absence of the strong thiol (ME-SH: 3.45 ppm) resonance confirmed a successful link between PAA and ME (6.2 NMR monomer reference). The NMR peaks of the polymerized ME corresponded to the peaks obtained from a similar telomerization with dimethylaminoethyl methacrylate and ME in literature [48, 50, 80]. The molecular weight was calculated by end group analysis through the ME methylene group (B2: 3.50 ppm), because no overlapping peak was observed. The number average molecular weight $M_{n\ H1\ NMR}$ was calculated as 2446 g/mol. This result was close to the expected 2000 g/mol for the synthesis.

After the polymerization the washing step in cold diethyl ether and drying in a vacuum oven was unsuccessful. The H1 NMR (Figure 19) showed remaining water (3.33 ppm), THF (1.76 ppm//3.60 ppm) and Toluene (2.30 ppm). The drying in the vacuum oven at 105 °C for 24 h did not remove the entrapped residual solvents from the polymer. Hydrogen bonding between water and carboxylic acid required 200 °C to break, which was observed in the TGA analysis. For future experiments the polymer should be purified through freeze drying before further use. The initiator AIBN also showed a strong peak (1.43 ppm) that needs to be removed before further processing of PAA-OH.

PAA-OH_{2K} was used as macroinitiator for the ROP in bulk with stannous octoate, GA and LA. From visual observation and H1 NMR (Figure 20) PAA-OH_{2K} did not melt at 130°C in the reaction vessel. It was assumed that PLGA synthesis was not initiated from the hydroxyl groups of PAA-OH_{2K} and bare PLGA was formed. Both characteristic PAA resonances for the methanetriyl group (D: 2.21 ppm) and the methylene group (E: 1.51 ppm) were barely visible.

Instead, the end groups of the PLGA polymer were visible. The methylene group of GA (C: 4.11 ppm) and methanetriyl group of LA (4.21 ppm) showed a lower nuclei resonance due to an adjacent hydroxyl group instead of an ester. From the end group integrals, the average molecular weight of the PLGA was calculated as 2858 g/mol and a conversion of LA of 89 % was found. After the synthesis PAA was not soluble in THF suggesting crosslinking by uncontrolled free radical polymerization with the remaining AIBN. For a successful synthesis the macroinitiator PAA-OH_{2K} should be free of water. Since the monomer acrylic acid was not completely dehydrated, distillation of the monomer is proposed. Furthermore, freeze drying of the PAA-OH_{2K} is an option that should be used in further experiments. Ahmadi et. al. and Xue et. al. [48, 50] were able to synthesize PAA-OH without residual water and other solvents without using rigid cleaning procedures above. Both demonstrated the potential of the resulting amphiphilic polymer PAA-PL(G)A for drug loading and pH responsive release mechanism. Using FNP for drug loading and particle formation with PAA-PLGA has yet to be tested.

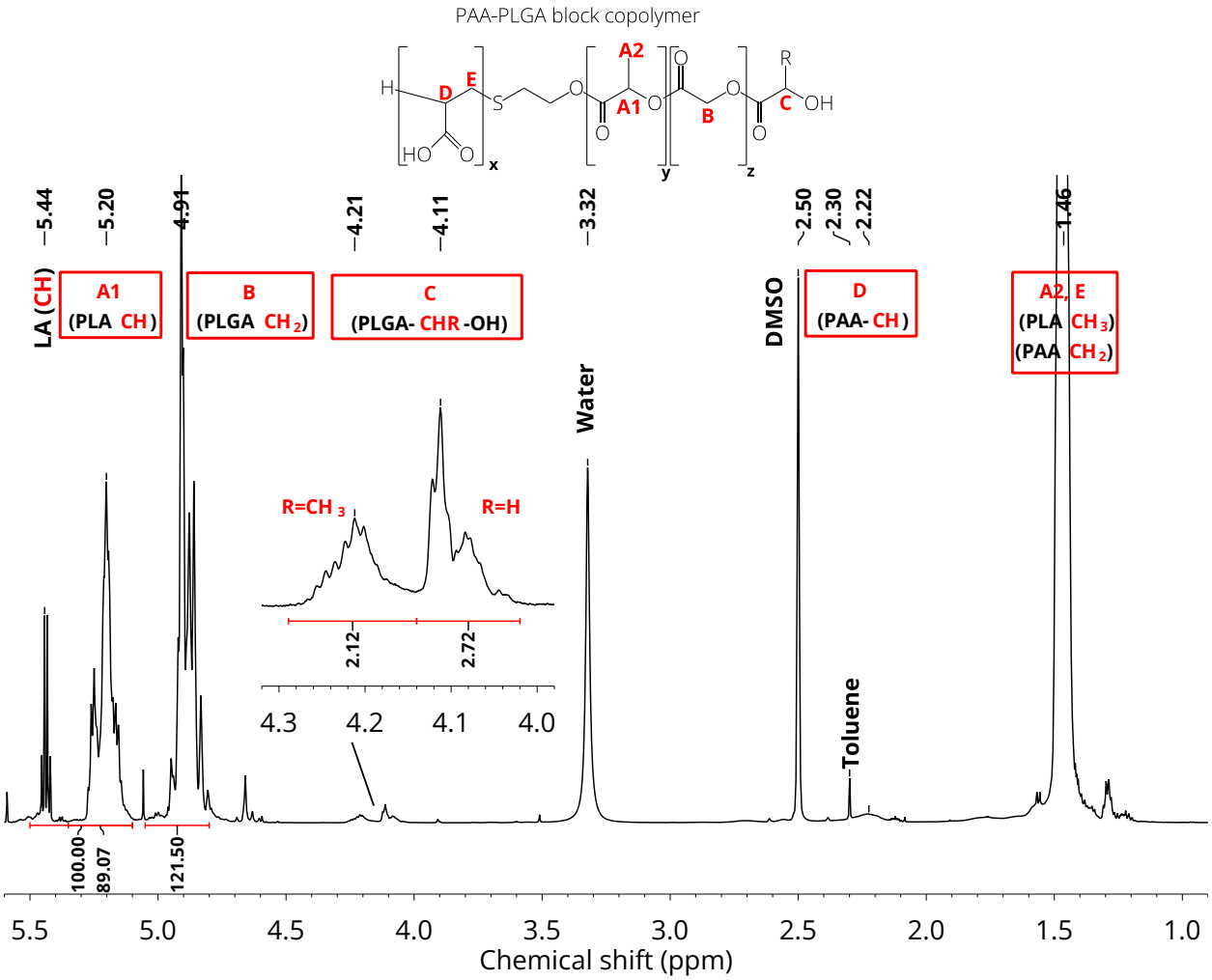

Figure 20: H1 NMR of PAA-PLGA; reaction unsuccessful, low PAA solubility (possibility of crosslinks).

4.5 Synthesis of PEG-PCL block-copolymer

Preliminary experiments of the PEG_{2K}-PCL_{2K} ROP synthesis with DBU showed degradation of the catalyst at a temperature of 90 °C. The solution changed dark brown 60 min into the polymerization and the conversion of CL to PCL was only 2 %. Change in temperature to 85 °C results in an increase in conversion to 42 % (Figure 21) over 22 h. The obtained solution was slightly yellow, suggesting some type of catalyst degradation. The NMR peaks of PEG_{2K}-PCL_{2K} were assigned to the peaks of PCL and CL (Figure 21) (6.2 NMR monomer reference) [81]. Depended on the location in polymer structure and adjacent groups the different methylene groups showed different proton resonances. For the end group analysis PEG (G: 3.52 ppm) was used. The linkage between PEG and PCL was confirmed by the PEG methylene group adjacent to PCL (F: 4.12 ppm). The total molecular weight for the polymer $M_{n\ H1\ NMR}$ was found as 2740 g/mol. The conversion of 42 % was calculated by the ratio of the two methylene groups of CL (ε: 4.21 ppm) and PCL (E: 3.99 ppm) adjacent to the ester bond. In Literature the polymerization conversion was reported to reach 95 % at 90 °C and 99 % at 100 °C for the copolymerization with PEG_{2K} [41]. Discoloration from oxidized DBU was reported. The total absence of Oxygen was required to avoid the early oxidization of the tertiary amine and deactivation of the catalyst [41]. The purging with nitrogen and the drying of PEG in the PEG_{2K}-PCL_{2K} synthesis might not be sufficient to remove all oxygen from the reaction vessel. The

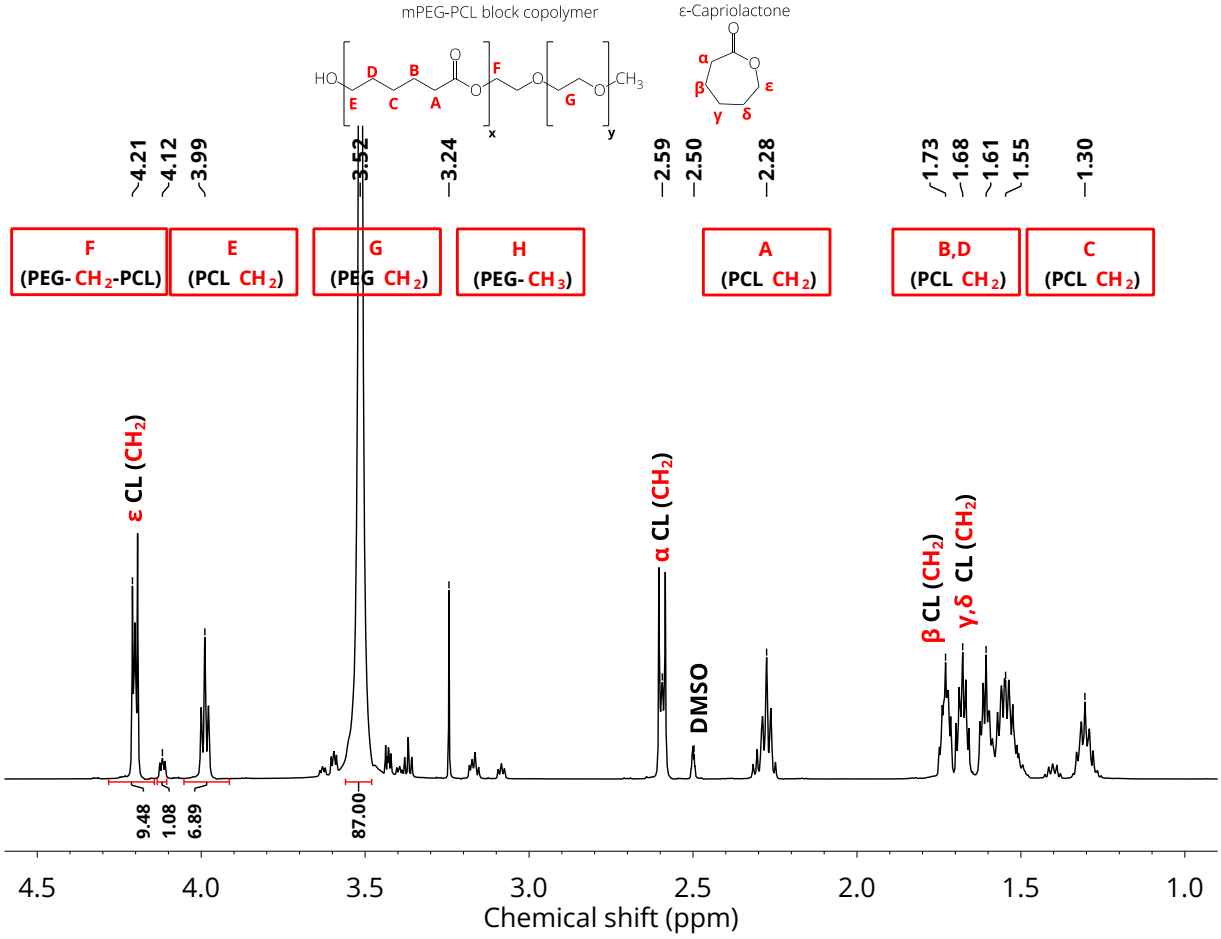

Figure 21: H1 NMR in *d6*-DMSO of PEG-PCL block-copolymers with 42% conversion of CL.

washing step of the polymer in cold diethyl ether did not result in precipitation and formation of suspension. A polymer powder could not be obtained. The PEG-PCL was used directly from the bulk with monomer CL still present.

4.6 Fabrication of NPs through FNP

For the fabrication of biocompatible NPs the previously produced Polymers PEG-PLA, PEG-PLGA, PEG-PCL, PAA-PLGA as well as commercial PLGA Resomer503H© were used in FNP. For the comparison between the different polymer samples the process parameters from the FNP setup were not varied. The flow rate of the aqueous phase was maximized to 100 mL/min with aqueous to organic ratio of 10 to 1. Supersaturation is maximized, while the mixing time (t_{mix}) is as short as possible. Tween80 was used with 0.1 v/v% in the aqueous phase to work as an additional stabilizer for the polymeric NPs. Since the critical micelle concentration (CMC) for Tween80® is 0.014 g*L^{-1}, micelles with~10 nm diameter are present in the solution [82]. Directly after the synthesis the particle hydrodynamic diameter was analyzed through DLS (Table 6). STEM grids were prepared for selected samples.

4.6.1 Bare polymeric NPs

All three ratios (1 : 5, 1 : 2, 1 : 1) of the block-copolymer PEG-PLA were analyzed from solution after the FNP process. PEG_{10K}-PLA_{10K} showed water solubility and did not form sterically stable NPs. The high ratio of hydrophilic and water-soluble PEG compared to hydrophobic PLA resulted in a low or no supersaturation condition during the high-speed mixing. For the higher ratio PEG_{2K}-PLA_{10K} and PEG_{5K}-PLA_{10K} NPs sized 41.2 ± 0.3 nm and 45.9 ± 1.7 nm were present in the MQ water/ THF mixture (Table 6). Similar sizes of NPs were reported with commercial, DBU and $Sn(Oct)_2$ based PEG-PLA block copolymers in CJI [35, 83] and MIVM [2] reactors. The NPs solution showed a zeta potential of -1.7 ± 0.7 mV. Literature suggests that PEG-PLA NPs are mostly electrostatically stabilized, due to instantaneous precipitation in saline water [2, 35]. The addition of salts affects the solubility of the PEG chains in water, resulting in lower solubility and increased aggregation behavior [84]. This was confirmed by STEM Images for PEG_{5K}-PLA_{10K} as particle underwent Ostwald ripening showing wide particle distribution.

The three ratios of the block copolymer PEG-$PL_{7.5K}G_{2.5K}$A were also used for the NPs fabrication through FNP. The glycolide added to the block copolymer increased the size of the resulting NPs to 64.6 ± 3.6 nm for PEG_{2K}-$PL_{7.5K}G_{2.5K}$A and 56.2 ± 3.5 nm for PEG_{5K}-$PL_{7.5K}G_{2.5K}$A. The high PEG ratio sample PEG_{10K}-$PL_{7.5K}G_{2.5K}$A with a GA sequence length of 5 did not dissolve properly in THF and could not be used for particle synthesis. The size increased of PEG-PLGA compared to PEG-PLA is connected to the increase in hydrophilicity for the Polymer containing the glycolide. Difference between PEG and PLGA hydrophilicity is smaller

compared to PEG to PLA. During the FNP mixing process the PEG-PLGA will have more time to incorporate polymers in the forming micelle before stabilized by a PEG corona. These assumptions have been applied for the stabilization and size explanation of coated hydrophobic drugs, but should be applicable for bare polymeric Nanoparticles [2, 35]. The zeta potential for PEG_{2K}-$PL_{7.5K}G_{2.5K}A$ was -7.6 ± 0.2 mV. The significantly higher zeta potential compared to PEG-PLA suggests a good PEG corona around the hydrophobic PLGA core stabilizing the particle. In STEM analysis the NPs were observed only by addition of PTA stain (Figure 22). Small Tween80 micelles ~10 nm were present on the stain grid as well. Through control experiments it was concluded that they are not affecting size of particles measured through DLS and STEM. Because of small size and low concentration of tween80 micelles, DLS was not able to pick up a signal around 10 nm.

The DBU catalyzed polymer PEG_{2K}-PCL_{2K} was also used for the synthesis of NPs by FNP. Since the conversion was only 42 % the length of the hydrophobic PCL block is short. DLS yielded a particle size of 18.4 ± 1.6 nm, suggesting a fast stabilization of the NPs (Table 6). Hydrophobic interaction to PEG-PCL molecules near a formed NPs are shielded by the long hydrophilic PEG changes forming a corona. Literature reports PEG_{2K}-PCL_{3K} to form 66 ± 15 nm sized NPs when mixed in 10 : 1 MQ water to THF and twice the polymer concentration in an MIVM reactor [85]. In this study lower polymer concentration and smaller hydrophobic block length were used. The resulting reduction in supersaturation and polymer -polymer interaction shows smaller NPs. This result should be taken with care as the residual monomer is present in the sample. Interaction between monomer and stabilizer/ polymer can influencing the NPs formation.

Table 6: Sizes of different Polymeric NPs produced by FNP. Organic phase: 1 wt% Polymer in THF. Aqueous phase: 0.1 v/v% Tween in MQ Water. DLS measurements ~1 hour after fabrication.

Polymer	Hydrodynamic radius (nm)	PDI	Stability
PEG_{2K}-PLA_{10K}	41.2 ± 0.3	18.4 ± 1.7	< 6 h
PEG_{5K}-PLA_{10K}	45.9 ± 1.7	23.4 ± 0.4	< 6 h
PEG_{5K}-PLA_{10K} + IONPs	71.5 ± 6.6	23.4 ± 1.1	< 6 h
PEG_{10K}-PLA_{10K}	-	-	H_2O soluble
PEG_{2K}-$PL_{7.5K}G_{2.5K}A$	64.6 ± 3.6	22.5 ± 1.1	> 72 h
PEG_{5K}-$PL_{7.5K}G_{2.5K}A$	56.2 ± 3.5	24.5 ± 0.9	> 72 h
PEG_{5K}-$PL_{7.5K}G_{2.5K}A$ + IONPs	70.1 ± 4.3	20.3 ± 0.6	> 72 h
PEG_{10K}-$PL_{7.5K}G_{2.5K}A$	-	-	THF insoluble
PAA_{2K}-$PL_{2K}G_{1K}A$	163.4 ± 8.2	23.4 ± 1.7	> 72 h
PEG_{2K}-PCL_{2K}	18.4 ± 1.6	23.3 ± 0.3	N/A
PLGA Resomer503H©	143.0 ± 6.0	21.0 ± 3.5	> 30 days

The copolymerization of hydroxyl terminated PAA with PLGA catalyzed by $Sn(Oct)_2$ was unsuccessful. Nevertheless, the obtained homopolymer PLGA was used in FNP for comparison with commercial Resomer503H PLGA and the previously discussed copolymers. For the PLGA homopolymers a size of 163.4 ± 8.2 nm (PAA-PLGA) and 143.0 ± 6.0 nm (Resomer503H® PLGA) were obtained from the DLS measurements (Table 6). The similar sizes are achieved by using the same polymer concentration during the FNP run. Molecular weight 22471 g/mol (Resomer503H) and 1400 g/mol (PAA-PLGA) has an inferior influence on the resulting size of polymeric NPs. The hydrophobic PLGA grows by polymer-polymer addition from nearby PLGA molecules until the core is stabilized by the Tween80 block-copolymer. The sizes for the homopolymers are generally larger compared to the block-copolymer PEG-PLA and PEG-PLGA. For homopolymer the aggregation time (t_{ag}) is larger than the mixing time (t_{mix}) and an increase in size is obtained.

4.6.2 IONPs coated PEG-PL(G)A

For the FNP experiment 0.05 wt% oleic acid coated IONPs (13 ± 2 nm) are added with 1 wt% PEG_{5K}-$PL_{7.5K}G_{2.5K}A$ or PEG_{5K}-PLA_{10K} to the organic THF phase. FNP was performed following same parameters as for bare polymeric NPs. The average hydrodynamic radius for both polymers increased by ~20 nm upon addition of IONPs. STEM images showed that between 0-2 NPs were attached to the outside of a single stained PEG-PL(G)A particles (Figure 22). This could suggest that the mixture time (t_{mix}) during the FNP process was too fast. The hydrophobic IONPs were stabilized by addition of polymers and surfactant before the NPs can grow by further addition through polymer-polymer interactions. Control experiments showed that running IONPs in FNP without block-copolymers resulted in large agglomerations on the STEM grid. The block-copolymers played a crucial role in in the dispersion and stability of the IONPs during FNP.

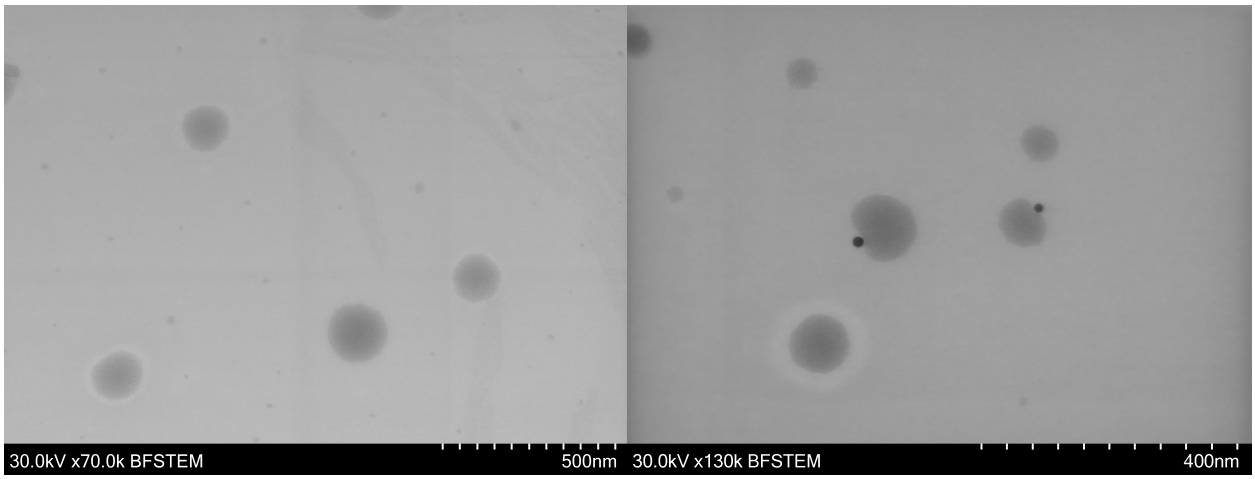

Figure 22: Hydrophilic polymeric Nanoparticles PEG_{5K}-$PL_{7.5K}G_{2.5K}A$ stained with 1 wt% PTA solution; bare polymeric NPs (left), Oleic acid IONPs + polymeric NPs (right).

The literature that has been reported on the incorporation of oleic acid coated IONPs into a polymeric NP uses the CJI reactor geometry [1, 67]. The coating is a result of a longer mixing time compared to MIVM allowing aggregation around the IONPs through polymer – polymer, polymer - IONPs and IONPs – IONPs interaction. Fuller et all. was able to coat multiple IONPs with a layer of PEG-PLA polymer resulting in sizes of 50-70 nm [1].

4.6.3 Investigation of PEG-PL(G)A NPs Stability

The stability of PEG_{5K}-$PL_{7.5K}G_{2.5K}A$ and PEG_{5K}-PLA_{10K} with and without IONPs was observed over a time span of 72 h (Figure 23). For bare PEG_{5K}-PLA_{10K} NPs the hydrodynamic size increased by 150 nm in the first 6 h after the FNP process. The instantaneous size increase indicates instability and fast Ostwald ripening of the polymeric NPs. Analog behavior of PEG-PLA block copolymers have been reported previously with particle stability of few hours [2, 35] The solubility of the PEG in PLA is extremely high as shown through solubility parameters presented in Literature [2, 35, 38]. Trapped hydrophilic PEG domains inside the hydrophobic PLA were present. Diffusion of these PEG domains to the surface destabilized the polymer. Lowering the molecular weight of the hydrophilic block to PEG_{2K}-PLA_{10K} did show similar instability. The Polydispersity (PDI) measured by DLS increased significantly from 23.4 ± 0.4 to over 30 with the proceeding Ostwald ripening process of the polymeric NPs. When IONPs were added to the organic phase the size increase of PEG_{5K}-PLA_{10K} NPs was with 75 nm significantly smaller in the same time interval. As observed earlier the IONPs, which attach to the outside of the NPs could hinder the Ostwald ripening process and contribute to the particle stability. This theory is supported by the PDI measurement were the IONPs PEG_{5K}-PLA_{10K} did a much smaller peak broadening over time.

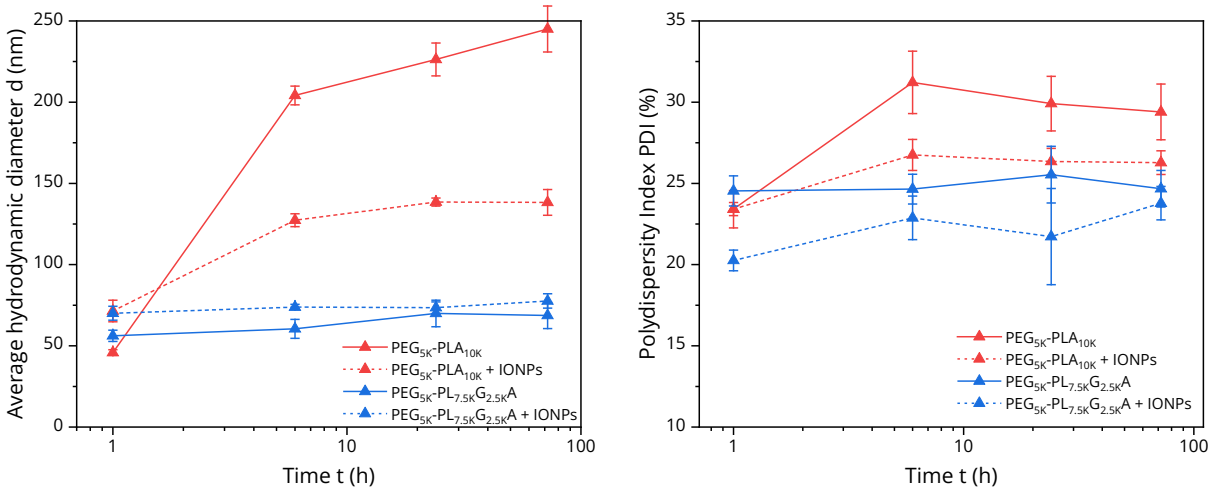

Figure 23: Stability of PEG-PLA vs PEG-PLGA NPs over time; Addition of IONPs increase the size and stability of the polymeric NPs.

The bare PEG_{5K}-$PL_{7.5K}G_{2.5K}$A polymeric NPs showed a more stable behavior over the course of 72 h compared to PEG-PLA (Figure 23). The hydrodynamic size of the particles increased by 10 nm with higher standard derivations for older samples. The structural change of the polymer by addition of the glycolide effected properties like solubility and hydrophilicity. The PLGA solubility in PEG is much lower compared to the PEG-PLA polymer, when described through the Hoy solubility parameter [2, 35, 38]. The number of PEG domains inside the polymer core was reduced, diffusion of PEG and water was avoided, and stability increased. When using lower molecular weight PEG_{2K} the particles were also stable throughout the first 72 h. The PDI of the polymeric NPs stayed constant over the time of 72 h. Ostwald ripening did not occur. Through the addition of the IONPs the stability of the NPs was preserved. Particle sizes of 70 nm and a PDI between 20-23 is measured for all time points. The particles PEG_{5K}-$PL_{7.5K}G_{2.5K}$A sizes were measured after 3 weeks of storage in the fridge and no significant size change is found. Both polymeric NPs PEG-PLGA and PEG-PLA were not stable when ultrasonication was used. Particles destabilize and form aggregates instantaneously.

PLGA homopolymers showed higher stability and resistance to ultrasonication compared to the block copolymers polymerized in this work. Experiments show that the sizes of the homopolymers are stable for more than 30 days. The hydrophobic PLGA core is mainly stabilized in suspension by a layer of Tween80. The driving force for Tween80 to assemble on the surface of the hydrophobic domain is high. Hydrophilic PEG domains are not incorporated in the core and Ostwald ripening is not favored.

From a stability point of view PEG-PLGA shows superior properties compared to PEG-PLA. PLGA homopolymer rely on the stabilization of the particles by a stabilizing agent, while the block copolymer of PEG-PLGA is stabilized by the polymer directly.

5. Conclusion

In this study, biocompatible amphiphilic block-copolymers suitable for biomedical applications were synthesized. The selection of the organic catalyst DBU for solution-based ROP was based on its low inherent toxicity. PEG-PLA and PEG-PLGA polymers with varying ratios of hydrophilic to hydrophobic blocks were successfully polymerized. The chemical structure of the polymers was characterized using H1 NMR, and the sequence length of lactide and glycolide blocks was determined through C13 NMR. It was observed that high glycolide content limited the maximum molecular weight of PEG-PLGA polymer to approximately 20,000 g/mol due to early precipitation. Kinetic experiments revealed the importance of maintaining a catalyst to macroinitiator ratio of less than 1 : 1 for achieving narrow polydispersity and avoiding secondary reaction pathways.

Attempts were made to synthesize two other amphiphilic block-copolymers. However, the bulk synthesis of PEG-PCL using DBU as a catalyst at elevated temperature resulted in only 42 % conversion. Similarly, the synthesis of PAA-PLGA faced challenges in purifying PAA-OH due to hydrogen bonding between water and carboxylic acid groups.

These polymers were utilized in the fabrication of bare polymeric NPs through Flash FNP. The size of the NPs varied depending on the polymer type. Stability tests revealed that PEG-PLA NPs remained stable for only a few hours before experiencing Ostwald ripening and aggregation. In contrast, PEG_{5K}-$PL_{7.5K}G_{2.5K}A$ NPs exhibited excellent stability over multiple days.

PEG_{5K}-PLA_{10K} and PEG_{5K}-$PL_{7.5K}G_{2.5K}A$ were also combined with OA IONPs to explore the possibility of coating hydrophobic IONPs. However, instead of incorporating the IONPs into the polymeric NP structure, single IONP particles were found to be attached to the exterior of the polymeric NPs. This observation may be attributed to the short mixing time utilized in the FNP process, where the rapid nucleation and growth of polymeric NPs hindered the incorporation of IONPs within the hydrophobic domain. Nevertheless, the attachment of IONPs to the exterior of the polymeric NPs positively influenced their stability.

In future research, adjustments to the process parameters of FNP should be considered. These modifications could involve extending the mixing time or exploring the use of different solvents, which may enable the complete encapsulation of OA IONPs within the polymeric NPs. Furthermore, the incorporation of additional drugs into the NPs could create a theranostic carrier system, enhancing their potential biomedical applications.

6. Appendix

6.1 List of identified NMR peaks

Table 7: List of identified NMR peaks for PEG-PL(G)A in *d6*-DMSO (Reference Peaks: H1 DMSO 2.50 ppm).// C13 DMSO 40 ppm) [64].

Component	H1	Literature H1	C13	Literature C13
2-Propanol	1.04	[75]	25.56	[75]
Acetone	2.02	[75]	31.18	[75]
Chloroform			-	-
DMSO	2.50	[75]	40.00	[75]
glycolide (CH2)	5.05	[86]	65.78	-
glycolide (CO)	-	-	165.91	-
PGA (CH2)	4.91	[59, 86]	61.22	[87]
GG (CO)	-	-	167.18	[59, 63, 76]
GL (CO)	-	-	167.07	[59, 63, 76]
lactide (CH3)	1.47	[86]	15.59	-
lactide (CH)	5.44	[86]	72.7	-
lactide (CO)	-	-	169.01	-
PLA (CH3)	1.52	[59]	16.93	[87]
PLA (CH)	5.20	[59]	69.18	[87]
LL (CO)	-	-	169.67	[59, 63, 76]
LG (CO)	-	-	169.74	[59, 63, 76]
PEG (CH2)	3.51	[59, 86]	70.29	[87]
PEG-GG (CH2)	4.12	[59, 86]	-	-
PEG-LL (CH2)	4.22	[59, 86]	-	-
mPEG (OCH3)	3.24	[59, 86]	-	-
Water	3.33	[75]	-	-

6.2 NMR monomer reference spectra

glycolide in d6-DMSO (H1/C13): [64]

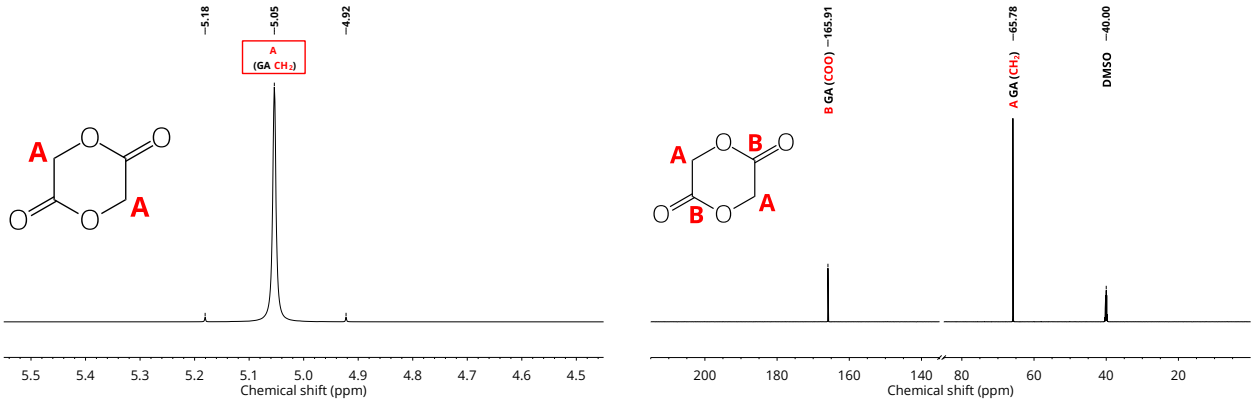

rac-Lactide in d6-DMSO (H1/C13): [64]

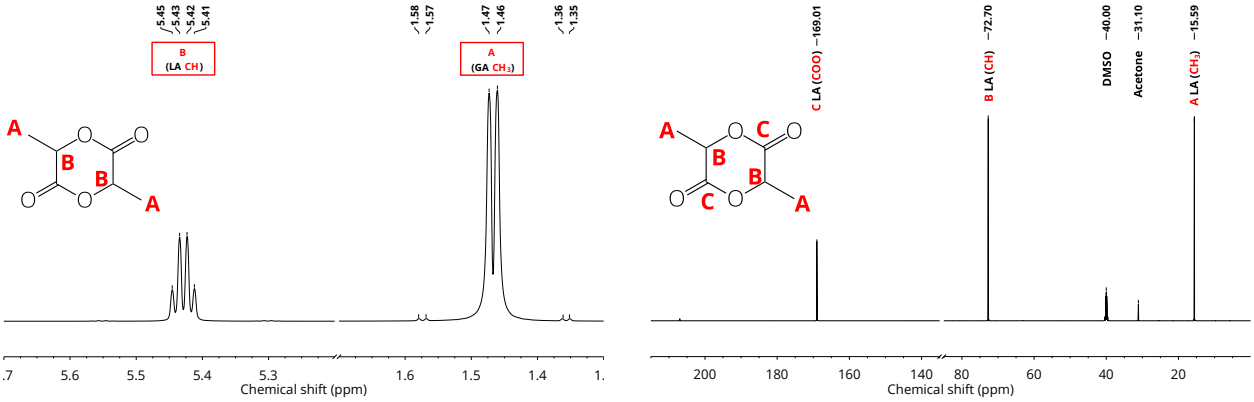

Acrylic Acid in d6-DMSO (H1):

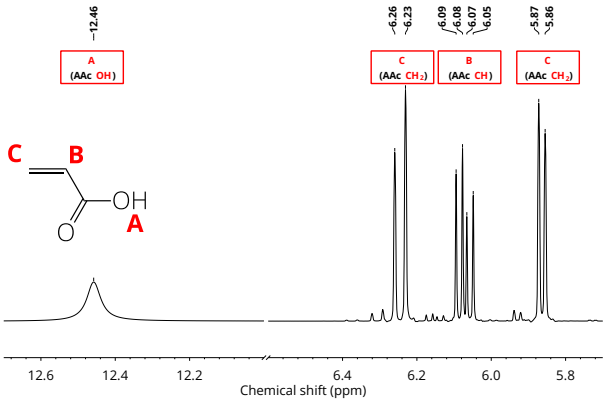

Mercaptoethanol in d6-DMSO (H1):

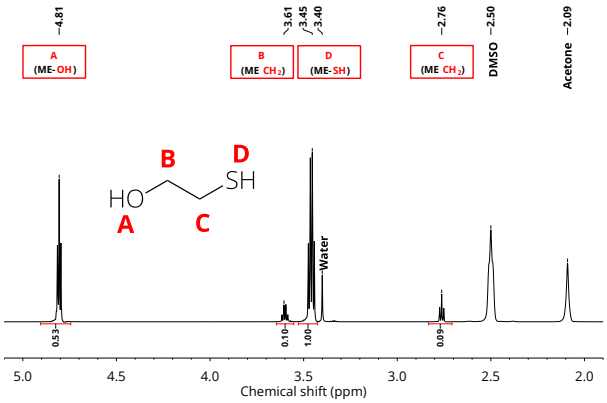

Caprolactone in d6-DMSO (H1):

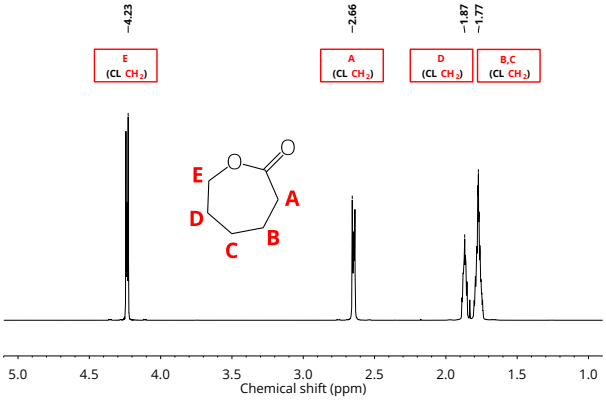

Figure 24: NMR reference spectra for Monomers: GA, LA, ME, AAc and CL.

6.3 NMR spectra of PEG-PL(G)A samples

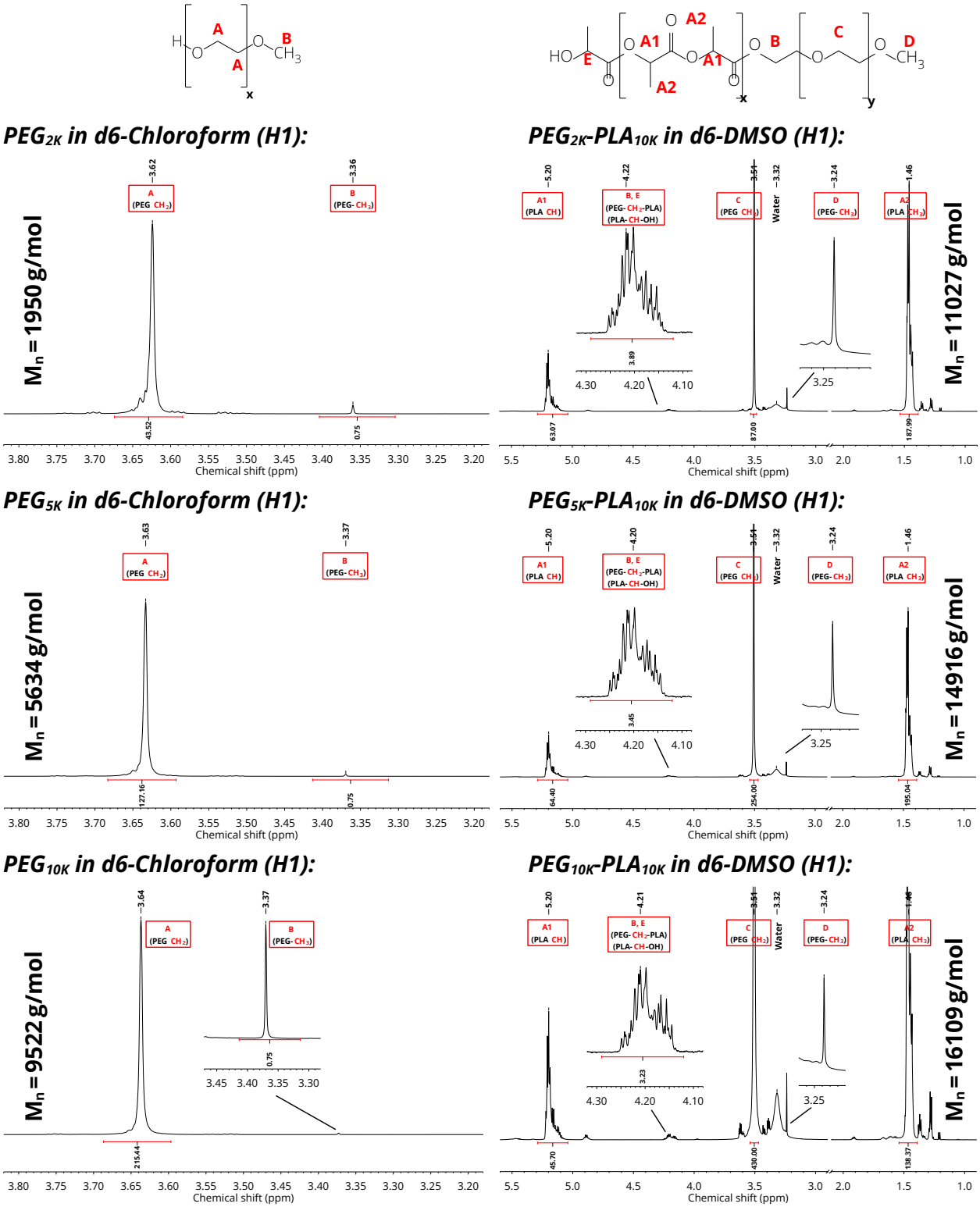

Figure 25: H1 NMR spectra of PEG and PEG-PLA with $M_{n\ H1\ NMR}$ molecular weight determination.

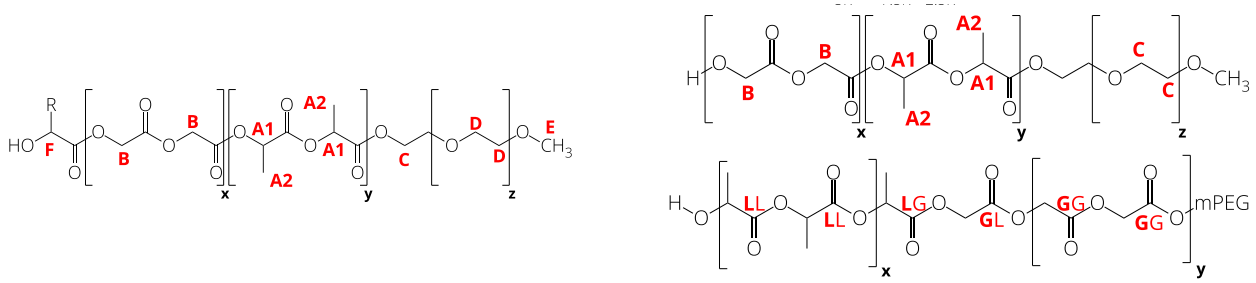

PEG_{2K}-$PL_{7.5K}G_{2.5K}$A in d6-DMSO (H1/C13):

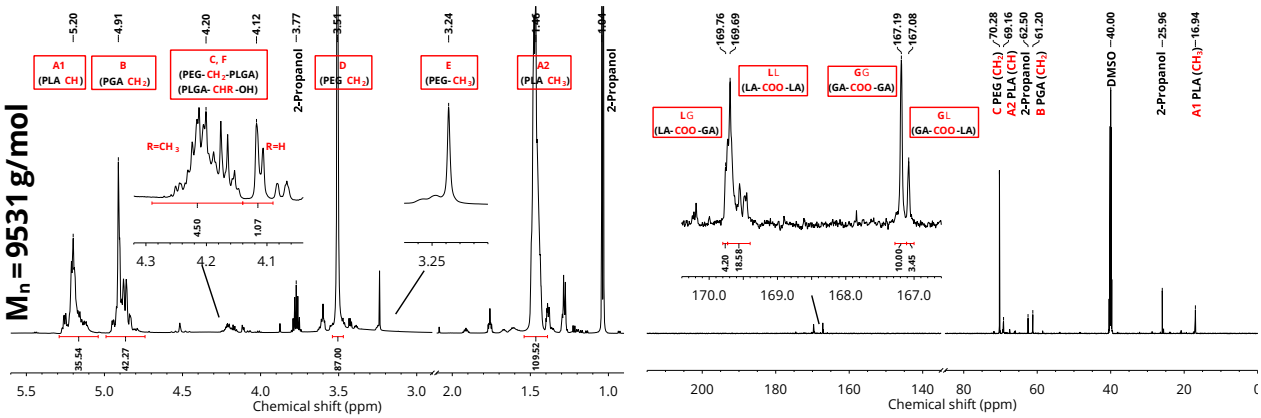

PEG_{5K}-$PL_{7.5K}G_{2.5K}$A in d6-DMSO (H1/C13):

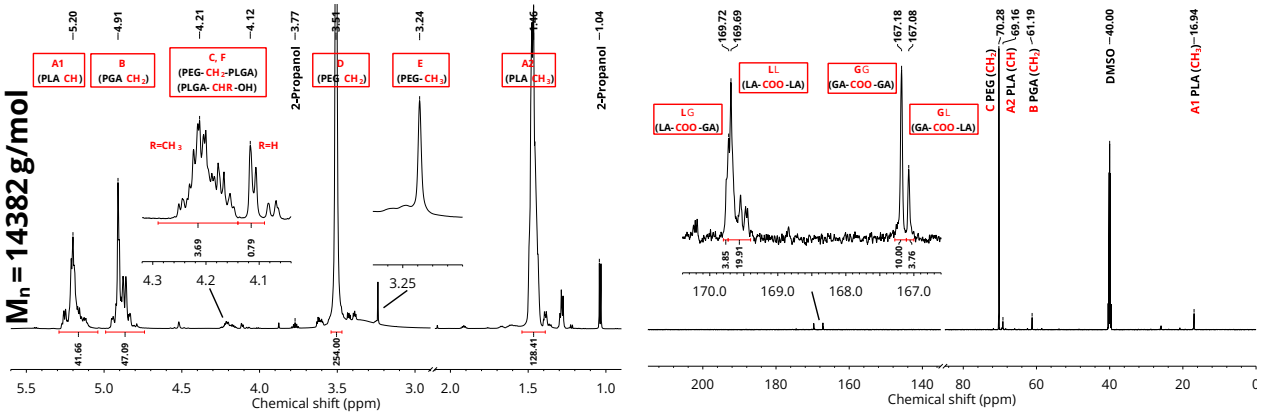

PEG_{10K}-$PL_{7.5K}G_{2.5K}$A in d6-DMSO (H1/C13):

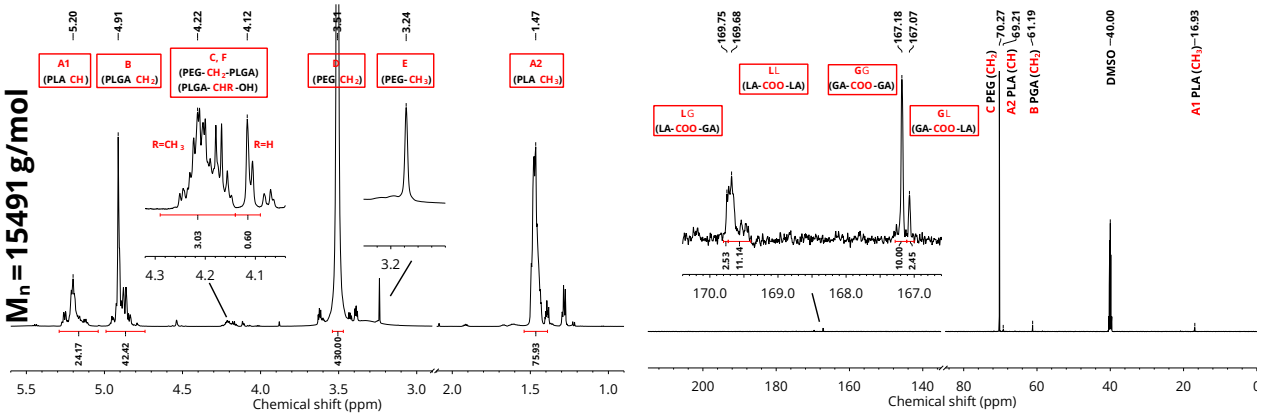

Figure 26: H1 NMR spectra of PEG-PLGA with $M_{n\ H1\ NMR}$ molecular weight determination; C13 NMR spectra of PEG-PLGA for sequence length determination.

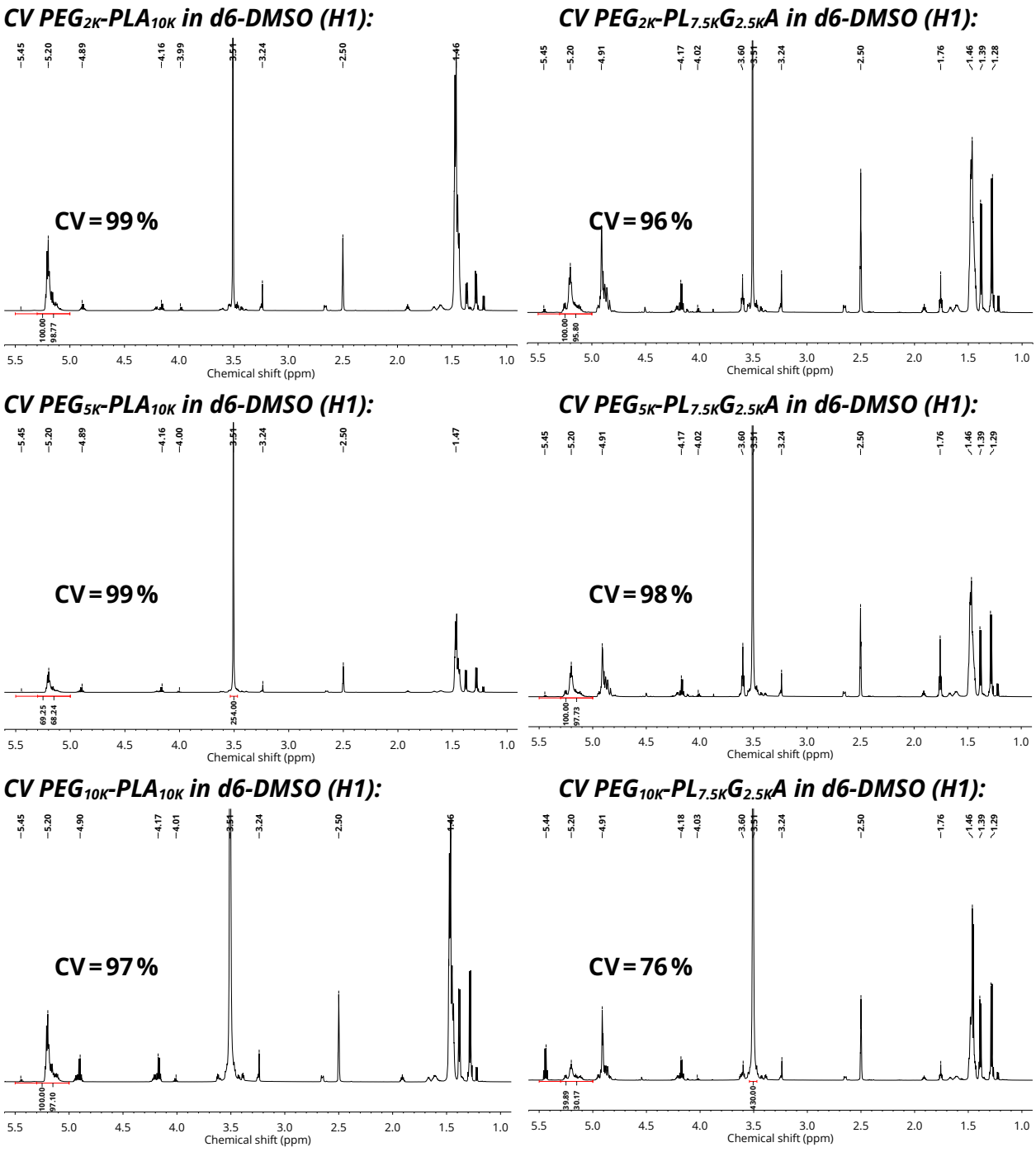

Figure 27: H1 NMR spectra of PEG-PLA and PEG-PLGA for conversion determination before washing and drying.

Number average molecular weight ($M_{n\ H1\ NMR}$) PEG_{5K}-$PL_{7.5K}G_{2.5K}A$

$$M_{n\ H1\ PEG_{5K}} = \frac{I_{PEG\ 5K\ CH_2}}{I_{PEG\ 5K\ CH_3}} * \frac{3}{4} * 44.05\frac{g}{mol} + 15\frac{g}{mol} + 18.02\frac{g}{mol} = 5634\frac{g}{mol} \quad (10)$$

$$M_{n\ H1\ PEG_{5K}-PL_{7.5K}G_{2.5K}A} = 5634\frac{g}{mol} + \frac{I_{PLA\ CH}}{I_{PEG\ CH_2}} * 2 * \frac{I_{PEG\ 5K\ CH_2}}{I_{PEG\ 5K\ CH_3}} * \frac{3}{4} * 144.13\frac{g}{mol} + \frac{I_{PGA\ CH}}{I_{PEG\ CH_2}} * \frac{I_{PEG\ 5K\ CH_2}}{I_{PEG\ 5K\ CH_3}} * \frac{3}{4} * 116.07\frac{g}{mol} = 14382\frac{g}{mol} \quad (11)$$

$$H1\ Molar\ Ratio\ GA{:}LA = \frac{0.5 * I_{\boldsymbol{PGA}}}{0.5 * I_{\boldsymbol{PGA}} + I_{\boldsymbol{PLA}}} = 36.1\% \quad (12)$$

Sequence length LA/GA PEG_{5K}-$PL_{7.5K}G_{2.5K}A$:

$$sequence\ length\ \overline{L_{LA}} = \frac{I_{LL}}{I_{LG}} + 1 = 6.17 \quad (13)$$

$$sequence\ length\ \overline{L_{GA}} = \frac{I_{GG}}{I_{GL}} + 1 = 3.66 \quad (14)$$

$$C13\ Molar\ Ratio\ GA{:}LA = \frac{\overline{L_{GA}}}{\overline{L_{LA}} + \overline{L_{GA}}} = 37.2\% \quad (15)$$

Conversion LA PEG_{5K}-$PL_{7.5K}G_{2.5K}A$ (before washing + drying):

$$CV\ LA = \frac{I_{PLA\ CH}}{I_{PLA\ CH} + I_{LA\ CH}} = 97.7\% \quad (16)$$

6.4 Raw Data Links:

Results raw data:

https://studntnu.sharepoint.com/:f:/s/o365_FunNanoResearchGroup-Fall2020HelenaSpecializationProject/EpMW8NYV6alDivgDx4s4OqYBPi3_9uTS162pYK24wNuMZQ?e=n3weTv

Presentations:

https://studntnu.sharepoint.com/:f:/s/o365_FunNanoResearchGroup-Fall2020HelenaSpecializationProject/Emmf3RFT6GdAl4X_hgMapB8By0-VJt_0Q5hoy_-jREq0HA?e=BZfdfV

Experimental Procedure:

https://studntnu.sharepoint.com/:f:/s/o365_FunNanoResearchGroup-Fall2020HelenaSpecializationProject/EndmyboW6T9Nts6jKGkwSygBbJAnUqIziGRXjnqMVp296w?e=7WmZfM

7. References

[1] E. G. Fuller *et al.,* "Externally Triggered Heat and Drug Release from Magnetically Controlled Nanocarriers," *ACS Appl. Polym. Mater.*, vol. 1, no. 2, pp. 211–220, 2019, doi: 10.1021/acsapm.8b00100.

[2] Z. Zhu, "Effects of amphiphilic diblock copolymer on drug nanoparticle formation and stability," *Biomaterials*, vol. 34, no. 38, pp. 10238–10248, 2013, doi: 10.1016/j.biomaterials.2013.09.015.

[3] L. Zhu, Z. Zhou, H. Mao, and L. Yang, "Magnetic nanoparticles for precision oncology: theranostic magnetic iron oxide nanoparticles for image-guided and targeted cancer therapy," *Nanomedicine*, vol. 12, no. 1, pp. 73–87, 2017, doi: 10.2217/nnm-2016-0316.

[4] I. Khan, K. Saeed, and I. Khan, "Nanoparticles: Properties, applications and toxicities," *Arabian Journal of Chemistry*, vol. 12, no. 7, pp. 908–931, 2019, doi: 10.1016/j.arabjc.2017.05.011.

[5] S. Mallakpour and C. M. Hussain, *Handbook of Consumer Nanoproducts*. Singapore: Springer Singapore; Imprint Springer, 2021.

[6] S. Moeinzadeh and E. Jabbari, "Nanoparticles and Their Applications," in *Springer Handbooks, Springer Handbook of Nanotechnology*, B. Bhushan, Ed., Berlin, Heidelberg: Springer Berlin Heidelberg, 2017, pp. 335–361.

[7] A. I. López-Lorente, B. M. Simonet, and M. Valcárcel, "Analytical potential of hybrid nanoparticles," *Analytical and bioanalytical chemistry*, vol. 399, no. 1, pp. 43–54, 2011, doi: 10.1007/s00216-010-4110-0.

[8] A. Majid, W. Ahmed, Y. Patil-Sen, and T. Sen, "Synthesis and Characterisation of Magnetic Nanoparticles in Medicine," in *Micro and Nanomanufacturing Volume II*, M. J. Jackson, Ed., Cham: Springer International Publishing AG, 2018, pp. 413–442.

[9] A. Lassenberger, A. Scheberl, A. Stadlbauer, A. Stiglbauer, T. Helbich, and E. Reimhult, "Individually Stabilized, Superparamagnetic Nanoparticles with Controlled Shell and Size Leading to Exceptional Stealth Properties and High Relaxivities," *ACS applied materials & interfaces*, vol. 9, no. 4, pp. 3343–3353, 2017, doi: 10.1021/acsami.6b12932.

[10] J. Tao, S. F. Chow, and Y. Zheng, "Application of flash nanoprecipitation to fabricate poorly water-soluble drug nanoparticles," *Acta pharmaceutica Sinica. B*, vol. 9, no. 1, pp. 4–18, 2019, doi: 10.1016/j.apsb.2018.11.001.

[11] B. K. Johnson and R. K. Prud'homme, "Flash NanoPrecipitation of Organic Actives and Block Copolymers using a Confined Impinging Jets Mixer," *Aust. J. Chem.*, vol. 56, no. 10, p. 1021, 2003, doi: 10.1071/CH03115.

[12] A. M. THAYER, "FINDING SOLUTIONS," *Chem. Eng. News Archive*, vol. 88, no. 22, pp. 13–18, 2010, doi: 10.1021/cen-v088n022.p013.

[13] P. Bhatt, S. Trehan, N. Inamdar, V. K. Mourya, and A. Misra, "Polymers in Drug Delivery: An Update," in *Applications of Polymers in Drug Delivery*, A. Misra, Ed., 2nd ed., San Diego: Elsevier, 2021, pp. 1–42.

[14] S. Bobbala, S. D. Allen, and E. A. Scott, “Flash nanoprecipitation permits versatile assembly and loading of polymeric bicontinuous cubic nanospheres,” *Nanoscale*, vol. 10, no. 11, pp. 5078–5088, 2018, doi: 10.1039/c7nr06779h.

[15] S. Allen, O. Osorio, Y.-G. Liu, and E. Scott, “Facile assembly and loading of theranostic polymersomes via multi-impingement flash nanoprecipitation,” *Journal of controlled release : official journal of the Controlled Release Society*, vol. 262, pp. 91–103, 2017, doi: 10.1016/j.jconrel.2017.07.026.

[16] L. L. Osorno, A. N. Brandley, D. E. Maldonado, A. Yiantsos, R. J. Mosley, and M. E. Byrne, “Review of Contemporary Self-Assembled Systems for the Controlled Delivery of Therapeutics in Medicine,” *Nanomaterials (Basel, Switzerland)*, vol. 11, no. 2, 2021, doi: 10.3390/nano11020278.

[17] B. Yang and J.-Z. Du, “Ultrasound-responsive Homopolymer Nanoparticles,” *Chin J Polym Sci*, vol. 38, no. 4, pp. 349–356, 2020, doi: 10.1007/s10118-020-2345-6.

[18] K. Zhang *et al.,* “PEG-PLGA copolymers: their structure and structure-influenced drug delivery applications,” *Journal of controlled release : official journal of the Controlled Release Society*, vol. 183, pp. 77–86, 2014, doi: 10.1016/j.jconrel.2014.03.026.

[19] A. Duro-Castano, J. Movellan, and M. J. Vicent, “Smart branched polymer drug conjugates as nano-sized drug delivery systems,” *Biomaterials science*, vol. 3, no. 10, pp. 1321–1334, 2015, doi: 10.1039/c5bm00166h.

[20] M. Chanda, *Introduction to Polymer Science and Chemistry: A Problem-Solving Approach, Second Edition,* 2nd ed. Hoboken: CRC Press, 2013. [Online]. Available: http://gbv.eblib.com/patron/FullRecord.aspx?p=1595253

[21] Y. Liu *et al.,* “Formulation of Nanoparticles Using Mixing-Induced Nanoprecipitation for Drug Delivery,” *Ind. Eng. Chem. Res.*, vol. 59, no. 9, pp. 4134–4149, 2020, doi: 10.1021/acs.iecr.9b04747.

[22] S. Iqbal, M. Blenner, A. Alexander-Bryant, and J. Larsen, “Polymersomes for Therapeutic Delivery of Protein and Nucleic Acid Macromolecules: From Design to Therapeutic Applications,” *Biomacromolecules*, vol. 21, no. 4, pp. 1327–1350, 2020, doi: 10.1021/acs.biomac.9b01754.

[23] S. D. Allen, S. Bobbala, N. B. Karabin, and E. A. Scott, “On the advancement of polymeric bicontinuous nanospheres toward biomedical applications,” *Nanoscale horizons*, vol. 4, no. 2, pp. 258–272, 2019, doi: 10.1039/c8nh00300a.

[24] J. Bugno, H.-J. Hsu, and S. Hong, “Tweaking dendrimers and dendritic nanoparticles for controlled nano-bio interactions: potential nanocarriers for improved cancer targeting,” *Journal of drug targeting*, vol. 23, 7-8, pp. 642–650, 2015, doi: 10.3109/1061186X.2015.1052077.

[25] M. J. Mitchell, M. M. Billingsley, R. M. Haley, M. E. Wechsler, N. A. Peppas, and R. Langer, “Engineering precision nanoparticles for drug delivery,” *Nature reviews. Drug discovery*, vol. 20, no. 2, pp. 101–124, 2021, doi: 10.1038/s41573-020-0090-8.

[26] A. A. H. Abdellatif and A. F. Alsowinea, “Approved and marketed nanoparticles for disease targeting and applications in COVID-19,” *Nanotechnology Reviews*, vol. 10, no. 1, pp. 1941–1977, 2021, doi: 10.1515/ntrev-2021-0115.

[27] J. K. Patra *et al.,* “Nano based drug delivery systems: recent developments and future prospects,” *Journal of nanobiotechnology*, vol. 16, no. 1, p. 71, 2018, doi: 10.1186/s12951-018-0392-8.

[28] R. Kammari, N. G. Das, and S. K. Das, “Nanoparticulate Systems for Therapeutic and Diagnostic Applications,” in *Emerging Nanotechnologies for Diagnostics, Drug Delivery and Medical Devices*: Elsevier, 2017, pp. 105–144.

[29] M. Beck-Broichsitter, E. Rytting, T. Lebhardt, X. Wang, and T. Kissel, “Preparation of nanoparticles by solvent displacement for drug delivery: a shift in the "ouzo region" upon drug loading,” *European journal of pharmaceutical sciences : official journal of the European Federation for Pharmaceutical Sciences*, vol. 41, no. 2, pp. 244–253, 2010, doi: 10.1016/j.ejps.2010.06.007.

[30] K. Y. Hernández-Giottonini *et al.,* “PLGA nanoparticle preparations by emulsification and nanoprecipitation techniques: effects of formulation parameters,” *RSC advances*, vol. 10, no. 8, pp. 4218–4231, 2020, doi: 10.1039/c9ra10857b.

[31] Y. Liu, C. Cheng, R. K. Prud’homme, and R. O. Fox, “Mixing in a multi-inlet vortex mixer (MIVM) for flash nano-precipitation,” *Chemical Engineering Science*, vol. 63, no. 11, pp. 2829–2842, 2008, doi: 10.1016/j.ces.2007.10.020.

[32] W. S. Saad and R. K. Prud’homme, “Principles of nanoparticle formation by flash nanoprecipitation,” *Nano Today*, vol. 11, no. 2, pp. 212–227, 2016, doi: 10.1016/j.nantod.2016.04.006.

[33] S. Bandyopadhyay, *Fabrication and Application of Nanomaterials,* 1st ed. New York, N.Y.: McGraw-Hill Education; McGraw Hill, 2019. [Online]. Available: https://www.accessengineeringlibrary.com/content/book/9781260132236

[34] N. M. Pinkerton *et al.,* “Single-Step Assembly of Multimodal Imaging Nanocarriers: MRI and Long-Wavelength Fluorescence Imaging,” *Advanced healthcare materials*, vol. 4, no. 9, pp. 1376–1385, 2015, doi: 10.1002/adhm.201400766.

[35] K. M. Pustulka *et al.,* “Flash nanoprecipitation: particle structure and stability,” *Molecular pharmaceutics*, vol. 10, no. 11, pp. 4367–4377, 2013, doi: 10.1021/mp400337f.

[36] H. Shen, S. Hong, R. K. Prud’homme, and Y. Liu, “Self-assembling process of flash nanoprecipitation in a multi-inlet vortex mixer to produce drug-loaded polymeric nanoparticles,” *J Nanopart Res*, vol. 13, no. 9, pp. 4109–4120, 2011, doi: 10.1007/s11051-011-0354-7.

[37] *Hansen solubility parameters: A user's handbook,* 2nd ed. Boca Raton: Taylor & Francis, 2007. [Online]. Available: https://ebookcentral.proquest.com/lib/kxp/detail.action?docID=300509

[38] *Hoy theory.* [Online]. Available: http://www.compchemcons.com/products/Hoy/hoy_theory.html (accessed: Jun. 12 2023).

[39] C. E. Markwalter and R. K. Prud'homme, “Design of a Small-Scale Multi-Inlet Vortex Mixer for Scalable Nanoparticle Production and Application to the Encapsulation of Biologics by Inverse Flash NanoPrecipitation,” *Journal of pharmaceutical sciences*, vol. 107, no. 9, pp. 2465–2471, 2018, doi: 10.1016/j.xphs.2018.05.003.

[40] N. J. Sherck, H. C. Kim, and Y.-Y. Won, “Elucidating a Unified Mechanistic Scheme for the DBU-Catalyzed Ring-Opening Polymerization of Lactide to Poly(lactic acid),” *Macromolecules*, vol. 49, no. 13, pp. 4699–4713, 2016, doi: 10.1021/acs.macromol.6b00621.

[41] Y. Chen *et al.,* “Reinvestigation of the ring-opening polymerization of ε-caprolactone with 1,8-diazacyclo[5.4.0]undec-7-ene organocatalyst in bulk,” *European Polymer Journal*, vol. 161, p. 110861, 2021, doi: 10.1016/j.eurpolymj.2021.110861.

[42] E. Marin, M. I. Briceño, and C. Caballero-George, “Critical evaluation of biodegradable polymers used in nanodrugs,” *International journal of nanomedicine*, vol. 8, pp. 3071–3090, 2013, doi: 10.2147/IJN.S47186.

[43] *Caelyx pegylated liposomal | European Medicines Agency.* [Online]. Available: https://www.ema.europa.eu/en/medicines/human/EPAR/caelyx-pegylated-liposomal#assessment-history-section (accessed: May 20 2023).

[44] *Onivyde pegylated liposomal (previously known as Onivyde) | European Medicines Agency.* [Online]. Available: https://www.ema.europa.eu/en/medicines/human/EPAR/onivyde-pegylated-liposomal (accessed: May 20 2023).

[45] E. Khodaverdi, M. Gharechahi, M. Alibolandi, F. S. M. Tekie, B. Z. Khashyarmanesh, and F. Hadizadeh, “Self-assembled supramolecular hydrogel based on PCL-PEG-PCL triblock copolymer and γ-cyclodextrin inclusion complex for sustained delivery of dexamethasone,” *International journal of pharmaceutical investigation*, vol. 6, no. 2, pp. 78–85, 2016, doi: 10.4103/2230-973X.177809.

[46] *Methoxy Polyethylene Glycol (mPEG) Manufacturing and Development Services | CDMO Company | CRO | Aurigene Pharmaceutical Services.* [Online]. Available: https://www.aurigeneservices.com/services/development-manufacturing/mpeg (accessed: May 19 2023).

[47] M. Gilbert, Ed., *Brydson's plastics materials*. Amsterdam: Butterworth-Heinemann is an imprint of Elsevier, 2017.

[48] E. Ahmadi *et al.,* “Enhanced anticancer potency by combination chemotherapy of HT-29 cells with biodegradable, pH-sensitive nanoparticles for co-delivery of hydroxytyrosol and doxorubicin,” *Journal of Drug Delivery Science and Technology*, vol. 51, pp. 721–735, 2019, doi: 10.1016/j.jddst.2019.03.003.

[49] Y. O. Mezhuev *et al.,* “Kinetics of radical telomerization of acrylic acid in the presence of 1-octadecanethiol,” *Pure and Applied Chemistry*, vol. 90, no. 11, pp. 1743–1754, 2018, doi: 10.1515/pac-2018-0601.

[50] Y.-N. Xue *et al.,* "Synthesis and self-assembly of amphiphilic poly(acrylic acid-b-dl-lactide) to form micelles for pH-responsive drug delivery," *Polymer*, vol. 50, no. 15, pp. 3706–3713, 2009, doi: 10.1016/j.polymer.2009.05.033.

[51] *Evonik: RESOMER® Biodegradable Polymers for Controlled Release - Evonik Industries.* [Online]. Available: https://healthcare.evonik.com/en/drugdelivery/parenteral-drug-delivery/parenteral-excipients/bioresorbable-polymers/standard-polymers (accessed: May 19 2023).

[52] C. Jérôme and P. Lecomte, "Recent advances in the synthesis of aliphatic polyesters by ring-opening polymerization," *Advanced drug delivery reviews*, vol. 60, no. 9, pp. 1056–1076, 2008, doi: 10.1016/j.addr.2008.02.008.

[53] O. Dechy-Cabaret, B. Martin-Vaca, and D. Bourissou, "Controlled ring-opening polymerization of lactide and glycolide," *Chemical reviews*, vol. 104, no. 12, pp. 6147–6176, 2004, doi: 10.1021/cr040002s.

[54] D. K. Gilding and A. M. Reed, "Biodegradable polymers for use in surgery—polyglycolic/poly(actic acid) homo- and copolymers: 1," *Polymer*, vol. 20, no. 12, pp. 1459–1464, 1979, doi: 10.1016/0032-3861(79)90009-0.

[55] A. Little *et al.,* "Synthesis of Poly(Lactic Acid-co-Glycolic Acid) Copolymers with High Glycolide Ratio by Ring-Opening Polymerisation," *Polymers*, vol. 13, no. 15, 2021, doi: 10.3390/polym13152458.

[56] A. Beletsi, L. Leontiadis, P. Klepetsanis, D. S. Ithakissios, and K. Avgoustakis, "Effect of preparative variables on the properties of poly(dl-lactide-co-glycolide)-methoxypoly(ethyleneglycol) copolymers related to their application in controlled drug delivery," *International journal of pharmaceutics*, vol. 182, no. 2, pp. 187–197, 1999, doi: 10.1016/S0378-5173(99)00058-7.

[57] P. K. Samantaray *et al.,* "Poly(glycolic acid) (PGA): a versatile building block expanding high performance and sustainable bioplastic applications," *Green Chem.*, vol. 22, no. 13, pp. 4055–4081, 2020, doi: 10.1039/D0GC01394C.

[58] A. P. Dove, "Metal-Free Catalysis in Ring-Opening Polymerization," in *Handbook of ring-opening polymerization*, P. Dubois, O. Coulembier, and J.-M. Raquez, Eds., Weinheim: Wiley-VCH, 2009, pp. 357–378.

[59] H. Qian, A. R. Wohl, J. T. Crow, C. W. Macosko, and T. R. Hoye, "A Strategy for Control of "Random" Copolymerization of Lactide and Glycolide: Application to Synthesis of PEG-b-PLGA Block Polymers Having Narrow Dispersity," *Macromolecules*, vol. 44, no. 18, pp. 7132–7140, 2011, doi: 10.1021/ma201169z.

[60] S. Patil, J. Yoo, and Y.-Y. Won, "Investigation of the Mechanisms and Kinetics of DBU-Catalyzed PLGA Copolymerization via a Full-Scale Population Balance Analysis," *Ind. Eng. Chem. Res.*, vol. 60, no. 41, pp. 14685–14700, 2021, doi: 10.1021/acs.iecr.1c03096.

[61] B. G. G. Lohmeijer *et al.,* "Guanidine and Amidine Organocatalysts for Ring-Opening Polymerization of Cyclic Esters," *Macromolecules*, vol. 39, no. 25, pp. 8574–8583, 2006, doi: 10.1021/ma0619381.

[62] D. Grijpma, A. Nijenhuis, and A. Pennings, “Synthesis and hydrolytic degradation behaviour of high-molecular-weight l-lactide and glycolide copolymers,” *Polymer*, vol. 31, no. 11, pp. 2201–2206, 1990, doi: 10.1016/0032-3861(90)90096-H.

[63] J. Sun, J. Walker, M. Beck-Broichsitter, and S. P. Schwendeman, “Characterization of commercial PLGAs by NMR spectroscopy,” *Drug delivery and translational research*, vol. 12, no. 3, pp. 720–729, 2022, doi: 10.1007/s13346-021-01023-3.

[64] Felix Bogdan, “Understanding the Coating of Iron oxide nanoparticles with block-copolymers in Flash Nanoprecipitation,” *Spezilization Project*, 2022.

[65] P. Grossen, D. Witzigmann, S. Sieber, and J. Huwyler, “PEG-PCL-based nanomedicines: A biodegradable drug delivery system and its application,” *Journal of controlled release : official journal of the Controlled Release Society*, vol. 260, pp. 46–60, 2017, doi: 10.1016/j.jconrel.2017.05.028.

[66] A. Dzienia *et al.,* “Studying the catalytic activity of DBU and TBD upon water-initiated ROP of ε-caprolactone under different thermodynamic conditions,” *Polym. Chem.*, vol. 10, no. 44, pp. 6047–6061, 2019, doi: 10.1039/C9PY01134J.

[67] M. Modak *et al.,* “Magnetic Nanostructure-Loaded Bicontinuous Nanospheres Support Multicargo Intracellular Delivery and Oxidation-Responsive Morphological Transitions,” *ACS applied materials & interfaces*, vol. 12, no. 50, pp. 55584–55595, 2020, doi: 10.1021/acsami.0c15920.

[68] *Sigma Aldrich: IR Spectrum Table.* [Online]. Available: https://www.sigmaaldrich.com/NO/en/technical-documents/technical-article/analytical-chemistry/photometry-and-reflectometry/ir-spectrum-table (accessed: Jun. 15 2023).

[69] D. K. Wang *et al.,* “FT-IR characterization and hydrolysis of PLA-PEG-PLA based copolyester hydrogels with short PLA segments and a cytocompatibility study,” *J. Polym. Sci. Part A: Polym. Chem.*, vol. 51, no. 24, pp. 5163–5176, 2013, doi: 10.1002/pola.26930.

[70] X. Y. D. Soo *et al.,* “Polyethylene glycol/polylactic acid block co-polymers as solid–solid phase change materials,” *SmartMat*, 2023, doi: 10.1002/smm2.1188.

[71] R. Ghasemi *et al.,* “mPEG-PLA and PLA-PEG-PLA nanoparticles as new carriers for delivery of recombinant human Growth Hormone (rhGH),” *Scientific reports*, vol. 8, no. 1, p. 9854, 2018, doi: 10.1038/s41598-018-28092-8.

[72] Z. Zhang *et al.,* “Synthesis and characterization of serial random and block-copolymers based on lactide and glycolide,” *Polym. Sci. Ser. B*, vol. 58, no. 6, pp. 720–729, 2016, doi: 10.1134/S1560090416060191.

[73] G. Kister, G. Cassanas, and M. Vert, “Morphology of poly(glycolic acid) by IR and Raman spectroscopies,” *Spectrochimica Acta Part A: Molecular and Biomolecular Spectroscopy*, vol. 53, no. 9, pp. 1399–1403, 1997, doi: 10.1016/S0584-8539(97)00039-1.

[74] M. A. Murcia Valderrama, R.-J. van Putten, and G.-J. M. Gruter, “PLGA Barrier Materials from CO2. The influence of Lactide Co-monomer on Glycolic Acid Polyesters,” *ACS Appl. Polym. Mater.*, vol. 2, no. 7, pp. 2706–2718, 2020, doi: 10.1021/acsapm.0c00315.

[75] *Sigma Aldrich: NMR Chemical Shifts of Impurities Charts.* [Online]. Available: https://www.sigmaaldrich.com/NO/en/technical-documents/technical-article/analytical-chemistry/nuclear-magnetic-resonance/1h-nmr-and-13c-nmr-chemical-shifts-of-impurities-chart (accessed: Dec. 16 2022).

[76] Q. Gao, P. Lan, H. Shao, and X. Hu, "Direct Synthesis with Melt Polycondensation and Microstructure Analysis of Poly(L-lactic acid-co-glycolic acid)," *Polym J*, vol. 34, no. 11, pp. 786–793, 2002, doi: 10.1295/polymj.34.786.

[77] S. V. Ebadi *et al.,* "Immobilization of acetylcholinesterase on electrospun poly(acrylic acid)/multi-walled carbon nanotube nanofibrous membranes," *RSC Adv.*, vol. 5, no. 53, pp. 42572–42579, 2015, doi: 10.1039/C5RA03456F.

[78] A. R. Greenberg and I. Kamel, "Kinetics of anhydride formation in poly(acrylic acid) and its effect on the properties of a PAA-alumina composite," *J. Polym. Sci. Polym. Chem. Ed.*, vol. 15, no. 9, pp. 2137–2149, 1977, doi: 10.1002/pol.1977.170150908.

[79] *Sigma Aldrich: IR Spectrum Table.* [Online]. Available: https://www.sigmaaldrich.com/NO/en/technical-documents/technical-article/analytical-chemistry/photometry-and-reflectometry/ir-spectrum-table (accessed: May 17 2023).

[80] C. Boyer, G. Boutevin, J. J. Robin, and B. Boutevin, "Study of the telomerization of dimethylaminoethyl methacrylate (DMAEMA) with mercaptoethanol. Application to the synthesis of a new macromonomer," *Polymer*, vol. 45, no. 23, pp. 7863–7876, 2004, doi: 10.1016/j.polymer.2004.09.020.

[81] W. Peng *et al.,* "Oral delivery of capsaicin using MPEG-PCL nanoparticles," *Acta pharmacologica Sinica*, vol. 36, no. 1, pp. 139–148, 2015, doi: 10.1038/aps.2014.113.

[82] Y. Bide, M. A. Fashapoyeh, and S. Shokrollahzadeh, "Structural investigation and application of Tween 80-choline chloride self-assemblies as osmotic agent for water desalination," *Scientific reports*, vol. 11, no. 1, p. 17068, 2021, doi: 10.1038/s41598-021-96199-6.

[83] S. F. Chow, C. C. Sun, and A. H. L. Chow, "Assessment of the relative performance of a confined impinging jets mixer and a multi-inlet vortex mixer for curcumin nanoparticle production," *European journal of pharmaceutics and biopharmaceutics : official journal of Arbeitsgemeinschaft fur Pharmazeutische Verfahrenstechnik e.V*, vol. 88, no. 2, pp. 462–471, 2014, doi: 10.1016/j.ejpb.2014.07.004.

[84] R. Sadeghi and F. Jahani, "Salting-In and Salting-Out of Water-Soluble Polymers in Aqueous Salt Solutions," *J. Phys. Chem. B*, vol. 116, no. 17, pp. 5234–5241, 2012, doi: 10.1021/jp300665b.

[85] S. M. D'Addio *et al.,* "Effects of block copolymer properties on nanocarrier protection from in vivo clearance," *Journal of controlled release : official journal of the Controlled Release Society*, vol. 162, no. 1, pp. 208–217, 2012, doi: 10.1016/j.jconrel.2012.06.020.

[86] TUIJA ALANKO, *SYNTHESIS OF BIODEGRADABLE AND BIOCOMPATIBLE POLYMERS FOR DRUG DELIVERY APPLICATIONS*. Tampere University of Technology, 2016.

[87] Y. Yu, Z. Pang, W. Lu, Q. Yin, H. Gao, and X. Jiang, “Self-assembled polymersomes conjugated with lactoferrin as novel drug carrier for brain delivery,” *Pharmaceutical research*, vol. 29, no. 1, pp. 83–96, 2012, doi: 10.1007/s11095-011-0513-7.